August 2021

Estimating Thermonuclear Supernovae Rates in the Local Universe

Brianne Dunn
Clemson University, breegd@gmail.com

Estimating Thermonuclear Supernovae Rates in the Local Universe

---

A Thesis
Presented to
the Graduate School of
Clemson University

In Partial Fulfillment
of the Requirements for the Degree
Master of Science
Physics

---

by
Brianne Dunn
August 2021

Accepted by:
Dr. Mark Leising, Committee Chair
Dr. Dieter Hartmann
Dr. Stephen Kaeppler

Abstract

Type Ia supernovae (SNe Ia), otherwise known as thermonuclear supernovae, are objects in astronomy whose importance cannot be understated. They are essential to describing galaxy chemical evolution and abundances, and are the primary produces of iron and other iron group elements in the Universe. They inject energy into the interstellar medium (ISM), triggering bursts of star formation and effecting the kinematics of the ISM. Most importantly, the homogeneity between 'normal' SNe Ia light curve evolution and peak brightness after empirical corrections are applied has allowed these objects to be used in cosmology as high redshift distance indicators, leading to the discovery of the acceleration of the expanding Universe. Despite the importance of these objects, the progenitor systems and explosion mechanism leading up to a SN Ia explosion are not well understood. Observations in the gamma-ray regime will be able to probe the inner mechanisms of these events, providing valuable information on how these objects detonate and other fundamental physical properties. Prospective gamma-ray detectors focused on SN Ia physics have been proposed but understanding SN Ia rates are crucial to the future of these missions. In particular, local rates are useful to discern how many SNe Ia are expected to occur nearby within the average duration of a gamma-ray observatory.

Multiple methods have been used to derive the SN Ia rate at the local and cosmic level, but they often suffer from observational bias in that they are extrapolated from surveys that target pre-selected galaxies or specific areas of the sky. These rates may not provide an accurate description of the local Universe based on the actual distribution of galaxies and their physical properties.

In this work, we aim to describe the local SN Ia rate by applying a rate-size relation to all of the locally ($\leq$ 100 Mpc) cataloged galaxies. We calculate the SN rate for each galaxy based on its B-band luminosity and determine the probability of a SNe Ia event over the span of ten years, or the typical duration of a gamma-ray mission. We simulate SNe Ia within the local Universe and

investigate the rate of events based on the average number of SNe Ia for each run of the simulation. We find that approximately 89 SNe Ia per year are expected to occur within 100 Mpc. We also investigate our SNe rates as a function of distance and find that, in general, the frequency of SNe Ia over distance follows a trendline of form ad^3 where d is distance and a is a scale factor added to fit to the data.

Dedication

This work is dedicated to all of my family and friends whose support, motivation, and pestering kept me on track and made this thesis possible. Thank you to my mom and dad who have truly supported me my entire life and to my sisters for putting up with years of talk about space and stars. Thank you to my grandparents who were always interested in what I was working on. Thank you to all of my friends who constantly asked me questions and kept me on track. Thank you to my fur babies who I could always count on for a much needed cuddle when things got hard. And last but not least, thank you to my partner, my person, who was there through this entire project and helped me through the ups and downs of it all, the good and the not so good times. Thank you for your endless support and I love you all.

Acknowledgments

I would like to thank all the people at Clemson who helped me complete this thesis. Thank you to my advisor, Dr. Mark Leising, for helping me complete a thesis throughout an incredibly weird and uncertain year. Thank you to my committee, Dr. Dieter Hartmann and Dr. Stephen Kaeppler, for your patience and commentary on this project.

Table of Contents

List of Tables

List of Figures

Chapter 1

Introduction

Type Ia supernovae (SNe Ia), otherwise classified as thermonuclear supernovae, provide a wealth of knowledge to numerous areas of astronomy and physics. These transient events have played a critical role in determining the fundamental constants of our Universe. Their status as the the primary producers of iron and iron-group elements in the Universe makes them a key ingredient in determining the chemical composition and evolution of galaxies [Nomoto et al., 2013]. SNe Ia produce shock waves that inject energy into the interstellar medium (ISM), influencing star formation and galaxy evolution. The radioactive decay of the unstable elements produced during a SN Ia powers a light curve that exhibits exceptional homogeneity between events, and because of this standardizable nature, SNe Ia have been used as cosmological probes leading to the discovery of the expanding Universe [Riess et al., 1998, Perlmutter et al., 1999].

Due to their transient nature and the fact that the progenitor systems have yet to be identified, SNe Ia are difficult objects to interpret physically. Early time observations are limited as SNe are discovered only after their light curve reaches the limiting magnitude of detectors designed to survey the entire sky for transients. Simulations have difficulty identifying how a white dwarf star detonates and the type of burning front that reproduces the observed abundances of various elements. Many of these issues can be clarified through gamma-ray observations of SNe Ia events, specifically in the Mev range, as gamma-rays are more penetrating and have less complicated opacities compared to optical photons [Horiuchi and Beacom, 2010].

Detectors in the Mev nuclear gamma-ray regime have been proposed, although none are currently operating. Understanding the SNe Ia rate is essential to these proposed missions as an

accurate measure of the number of expected events will determine the practicality of a gamma-ray detector focused of SNe physics. SNe Ia rates have historically suffered from small sample sizes due to the limitations of detector sensitivity. Fortunately, their value to cosmology and other fields has lead to the inception of multiple SNe Ia studies designed to observe and catalog the events. Over the past several decades searches like the Lick Observatory Supernova Search (LOSS), Sloan Supernova Survey, and All-Sky Automated Survey for Supernova (ASAS-SN) have cataloged hundreds of SNe Ia in an effort to increase the number of observations and available data. Although more SN Ia events are cataloged, SNe Ia rates are often extrapolated from surveys that target pre-selected galaxies or certain portions of the sky, thus they may not provide an accurate measure of the rate based on the actual distribution of galaxies in the local Universe and their physical properties. Our goal in this thesis is to determine the local rate of SNe Ia as a function of the properties of nearby galaxies by applying a rate-size relation to all catalogued galaxies within 100 Mpc. Supernova rates per galaxy are low, so this is a Poisson-distributed process. We also aim to identify trends regarding the number of events based on their distance and location with a particular focus on how this information can be applied to prospective gamma-ray observatories.

We start with a review of the observational and physical properties of SNe Ia in chapter 2. Chapter 3 discusses our galaxy sample and the rate-size relation used to calculate the rate for individual galaxies within the local Universe, which we define as $\leq$100 Mpc for the purposes of this thesis. In chapter 4, we apply the rate relation to calculate the rate per galaxy, and with these rates simulate nearby SN Ia events. These simulated events are used to estimate the total rate over a ten year period, or the average duration of a gamma-ray observatory. Chapter 5 presents the results of our simulated SNe Ia rate calculation. We estimate the average number of events expected within 10 years. We also investigate the locations and distances of these events to identify if any areas are expected to contain more or less events based on the distribution of galaxies and their properties. The rate as a function of distance is estimated and fit to the cumulative event counts. We compare our results to the local rate densities to determine if they are accurate within statistics. Chapter 6 presents our conclusions.

Chapter 2

Thermonuclear Supernova Background

In this chapter, we provide a general review of type Ia supernovae. We describe the observational characteristics and what they imply about the physical properties of SNe Ia. We also review some of the main models for the progenitor systems and explosion mechanisms.

Thermonuclear supernovae, otherwise classified as Type Ia supernovae (SNe Ia), are the thermonuclear explosion of a carbon-oxygen white dwarf (WD) star in a binary system that has reached the Chandrasekhar limit (M $\approx 1.4 M_{\odot}$) through mass accretion. The term thermonuclear derives from the primary energy release mechanism, thermonuclear fusion.

During the runaway thermonuclear explosion, an order of 10^{51} ergs is released as kinetic energy. This process unbinds the star, launching the expanding ejecta to speeds of $\approx 10^4$ km s$^-$1, enriching the interstellar medium with much of its iron and iron group elements [Nomoto et al., 2013]. The decay of radioactive elements synthesized during the explosion, primarily the isotope nickel-56, powers the light curve of these objects. The optical light curves of normal SNe Ia reach very large magnitudes at peak brightness. Their luminosity at max light is standardizable through its relationship with the shape and decline rate of the light curve, therefore characterizing them as "standardizable" candles. This trait and the fact that their extreme brightness allows them to be observed at very large distances means they can be used as high redshift distance indicators [Jha et al., 2019]. These objects were used to discover that the expansion of the Universe was accel-

erating [Riess et al., 1998, Perlmutter et al., 1999] and to determine the much debated local Hubble constant [Riess et al., 2019].

Despite years of observational data available, the physical understanding of these objects remains a mystery. The progenitor system and explosion mechanism that produces the observed light curves and spectra are still uncertain, and an influx of data in recent years indicates that multiple progenitor channels are possible. Gamma-ray observations in the MeV range are crucial to answering these unknowns.

2.1 Observational Properties

The main source of information from SNe Ia comes from observations of their spectra and lightcurves. In this section, we review spectroscopic and photometric properties of "normal" SNe Ia and their host galaxy environments. We also mention the basic properties of "peculiar" SNe Ia, or observed events that do not follow the Philip's relation.

2.1.1 SNe Ia Spectral Properties

The spectra of a SN aids in identifying the various elements produced during the explosion, reveals the power source behind the observed light curve, and provides clues to the physical mechanisms of the event. Furthermore, correct classification of the various types of SNe relies heavily on the observed spectra of the object as photometric data is often not sufficient enough.

The historical classification of SNe Ia was first introduced by Minkowski (1941) in which he made the distinction between "type I" and "type II" supernovae based on whether or not the object's optical spectra showed signatures of hydrogen. [Elias et al., 1985] coined the term SN Ia to differentiate it from the SN Ib subclass, which displayed helium features in the near peak spectra. Modern classification schemes (see Filippenko, 1997 for a full review) define an SN Ia by a complete absence of hydrogen and helium lines and kinematically broadened and blueshifted ($\sim 10^3$ - 10^4 km s^{-1}) signatures of mainly silicon, iron, and calcium in the object's spectrum near peak brightness. The late-time spectrum further aids in classification in which blended emission lines of iron-group elements are observed [Filippenko, 1997].

The spectrum of a SN Ia evolves over the duration of the transient as various nucleosynthesis processes burn the core of the WD into intermediate-mass and iron group elements, with some

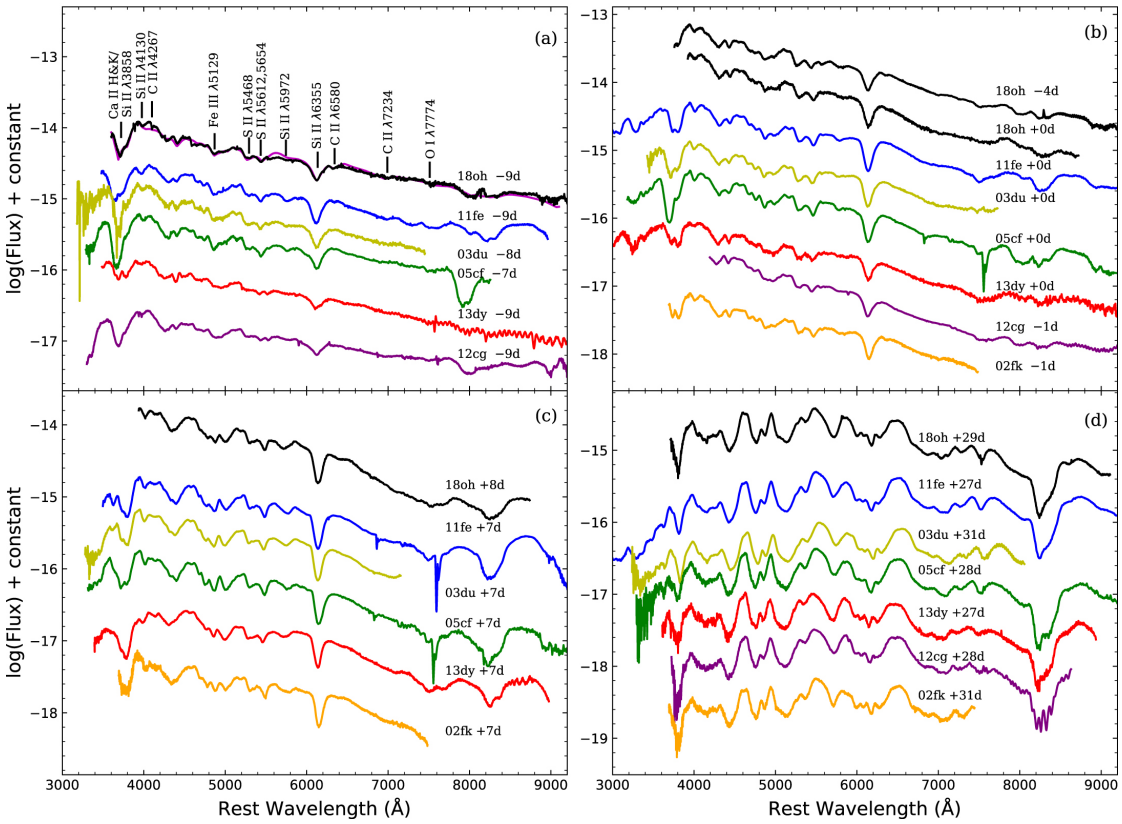

Figure 2.1: Spectra for various normal SNe Ia at t≈ -9 d, -4 d, 0d, and +1 month after peak B brightness corrected for reddening and redshift of the host galaxy. Note that the spectra have been arbitrarily shifted in the vertical direction for clarity. [Li et al., 2019]

residual carbon and oxygen leftover [Maoz et al., 2014]. Near peak brightness or "early-time phase," absorption lines from intermediate-mass elements dominate the spectrum. In particular, a very prominent Si II absorption line is found around 6100 Å as well as lines from O, S, Ca and blending of Fe-group elements [Gal-Yam, 2017].

The ejecta expand with time, becoming optically thin by ∼150 days past maximum light, at which point it enters its "nebular phase" [Silverman et al., 2013]. Iron-group elements become significant in the spectrum during this phase, with prominent features from forbidden emission lines of singly and doubly ionized iron and signatures of cobalt and nickel. Late-time observations of SN 2011fe indicate that after ∼1000 days, the spectrum shifts in ionization to primarily neutral iron. [Taubenberger et al., 2015].

It can be deduced from the evolution of the spectrum that ∼0.6 $M_\odot$ of radioactive ^{56}Ni is produced in a typical SN Ia explosion. The rest of the mass is distributed among stable iron-group

and intermediate-mass elements for a total ejecta mass around the Chandrasekhar mass, $M_{Ch} = 1.44\ M_{\odot}$ [Mazzali et al., 2007]. The synthesis of ^{56}Ni releases $\sim 1.1\times\ 10^{51}$ ergs from nuclear binding energy. Intermediate-mass elements release additional energy, providing a sufficient amount to overcome the gravitational binding energy of the CO WD ($\sim 0.5 \times 10^{51}$ ergs). Nucleosynthesis furthermore imparts kinetic energy to the ejecta, where typical observed SNe Ia ejecta velocities are 10^4 km s-1 [Maoz et al., 2014]. Arnett's law [Arnett, 1982] describes the proportionality between the bolometric luminosity at peak magnitude and the energy deposited by the decay of of ^{56}Ni. It provides an approximation of the mass of ^{56}Ni synthesized during a SN Ia.

2.1.2 SNe Ia Light Curves

Light curves have historically been one of the main sources of information regarding SNe and are still best studied in the optical band. They describe the change in magnitude, or brightness, over time. The zero-point of the light curve is traditionally defined by the B-band maximum and references to peak brightness refer to the peak magnitude observed in the B-band.

SN Ia light curves rise quickly to maximum, generally within 10 to 20 days. This is followed by a rapid decline ($\approx$ 3 mag) over the span of a month which then turns into a steady decline ($\approx$1 mag per 100 days) [Livio and Mazzali, 2018]. The Philip's relation [Phillips, 1993], or width vs peak-luminosity relation, describes the observed relationship between a SN Ia's peak magnitude and its subsequent decline rate. The original correlation related the B-magnitude decline through 15 days after maximum light, $\Delta m_{15}(B)$. The general trend is such that SNe Ia with brighter peak magnitudes show a slower decline rate in their light curves than those with lower peak magnitudes after maximum brightness. This relationship has been refined with larger SN Ia samples and has lead to the development of modern light curve fitters, furthering the use of SNe Ia as standardizable candles to measure distances, especially at high redshift. Empirical corrections must be made to the light curve for use in precision cosmology including corrections to the light curve shape or duration, the optical color at peak brightness, and corrections for the host galaxy properties [Jha et al., 2019].

The light curve of a SN Ia is primarily powered by the decay of ^{56}Ni produced during the event. Its behavior is dependent on the mass of ^{56}Ni synthesized, the kinetic energy of the explosion, and the opacity of the ejecta. ^{56}Ni has a half-life of 6.1 days and decays to ^{56}Co through electron capture. ^{56}Co decays primarily through electron capture (81%) and some β^+ decay (19%) with half-life of 77.3 days to stable ^{56}Fe. Gamma rays and positrons are emitted as decay products but are

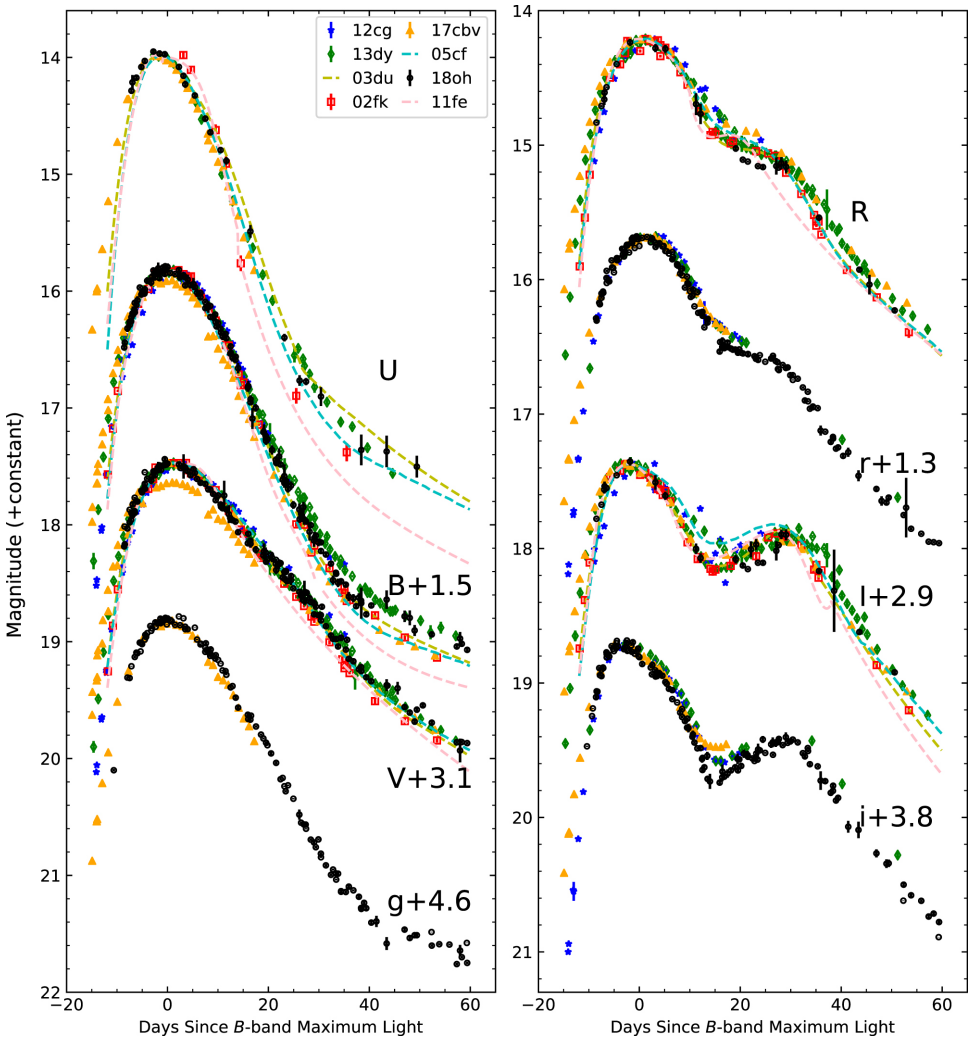

Figure 2.2: Optical light curves of various well observed normal SNe Ia, normalized to the peak magnitude of SN 2018oh. [Li et al., 2019]

quickly reprocessed by the optically thick ejecta to be emitted largely in the optical range. 85% of the luminosity from a SN Ia is observed between the U and I bands as gamma-ray photons deposit their energy on the ejecta through Compton scattering and are re-emitted. At early times, the opacity is primarily due to velocity broadened lines and incoherent scattering. As the ejecta expands and cools, gamma rays photons can more easily escape, providing another wavelength at which to study SN Ia physics. Gamma rays in particular can be used to probe the interior of the SN as they are more penetrating and and have much simpler opacities than optical photons [Maoz et al., 2014, Horiuchi and Beacom, 2010]. Unfortunately current detector sensitivities prevent robust studies of these objects in the MeV range, but proposed detectors seek to probe the high energy gamma-

ray regime and provide a better understanding of the physical mechanisms of thermonuclear SNe [Jha et al., 2019].

2.1.3 Host Galaxy Environments

Thermonuclear SNe are observed in all galaxy types and over a wide range of galactic environments varying in stellar masses, metallicities, and ages. This has significant consequences on the progenitor systems of SNe Ia in that they can form from both young and very old stellar systems. Studies have shown that correlations exist between the spectroscopic and photometric properties of SNe Ia and the global characteristics of the host galaxy such as its star formation rate (SFR), mass, metallicity, color, and stellar population age. In general, more luminous, and thus slower declining SNe Ia occur more often in later type galaxies (i.e. spiral galaxies), with lower mass, higher specific SFR, and younger stellar populations [Hakobyan et al., 2020]. The specific SN Ia rate (rate per unit stellar mass) depends on galaxy type too, and is observed to be higher in later type galaxies. Higher specific SN Ia rates are observed in bluer host galaxies compared to redder galaxies and in lower-mass galaxies compared to those with higher mass. This may be a consequence of the observed delay-time distribution (DTD). The DTD describes the time-dependant rate of SNe Ia following an instantaneous burst of star formation, and it peaks at younger progenitor ages. It decreases sharply with progenitor age, implying that SNe Ia are more common in younger systems but can occur in galaxies with very old stellar populations.

2.1.4 Thermonuclear SNe Zoo

Up until this point, we have described the properties of a 'normal' or standard SN Ia, an example being the well-observed SN 2011fe. Approximately two-thirds of all SN Ia events are categorized as normal and display photometric and spectroscopic characteristics similar to what we have described in the previous sections. For decades, the limited number of observations and incomplete data sets led to the idea that SN Ia events formed a spectroscopically homogeneous class with some light curve variations that in general follow the width vs peak luminosity relation. With the advancement of transient detectors and all-sky SN surveys, it is obvious that these thermonuclear events display a variety of photometric and spectroscopic properties, the result of which has led to the creation of multiple subclasses within the SN Ia classification scheme. In general, SNe Ia

that differ from the standard relations, specifically those that fall away from the width vs. peak luminosity relation, are termed 'peculiar,' and the various subclasses now make up what is known as the "thermonuclear SN zoo."

At one end of the peculiar SN Ia family lie the slow-declining, hot, luminous SN 1991T-like or SN 1999aa-like objects. These events are over luminous at B-band maximum by $\sim$0.6 mag compared to a normal SN Ia, and their near peak light spectra contain prominent Fe III and weak Si II features. On the opposite end lie the fast-declining, cool, subluminous SN 1991 bg-like objects which have a spectra characterized by intermediate-mass elements near peak light and unusually strong O I and Ti II lines post peak. Their luminosity is $\sim$2 mag less than that of a normal SN Ia. Even less luminous (more than 2 mag fainter than normal) are SNe Iax events which have early spectra resembling the 1991T-like SNe. Other peculiar thermonuclear transients include Ca-rich transients, super-Chandrasekhar SNe, and Sne Ia that show evidence of interaction with the circumstellar medium [Hakobyan et al., 2020].

The observed deviations from standard SN Ia properties has many consequences for the physical mechanisms of the explosion. The similarities between events within each subtype could indicate that multiple progenitor systems and/or different explosion mechanisms are at play. On the other hand, dispersion within the subtypes might arise from differences in abundance, metallicity, density, and temperature of the progenitor system. The fact that "transitional-type" SN Ia have been observed, showing overlaps between the subtypes, complicates SN Ia classification even more [Parrent et al., 2014]. All of these consequences signify that much work is still needed to be done to fully understand the physical mechanisms of thermonuclear SN. We review the physical models in the next section.

2.2 Physical Properties

As previously stated, the progenitor system of a SN Ia is not fully constrained and multiple models exist based on observational data. Here we review the two main models for a normal SN Ia progenitor, the single-degenerate (SD) and double-degenerate (DD) scenarios. Both models involve a binary system with a CO WD and a companion star, but differ on the nature of the companion. We also review the primary explosion models

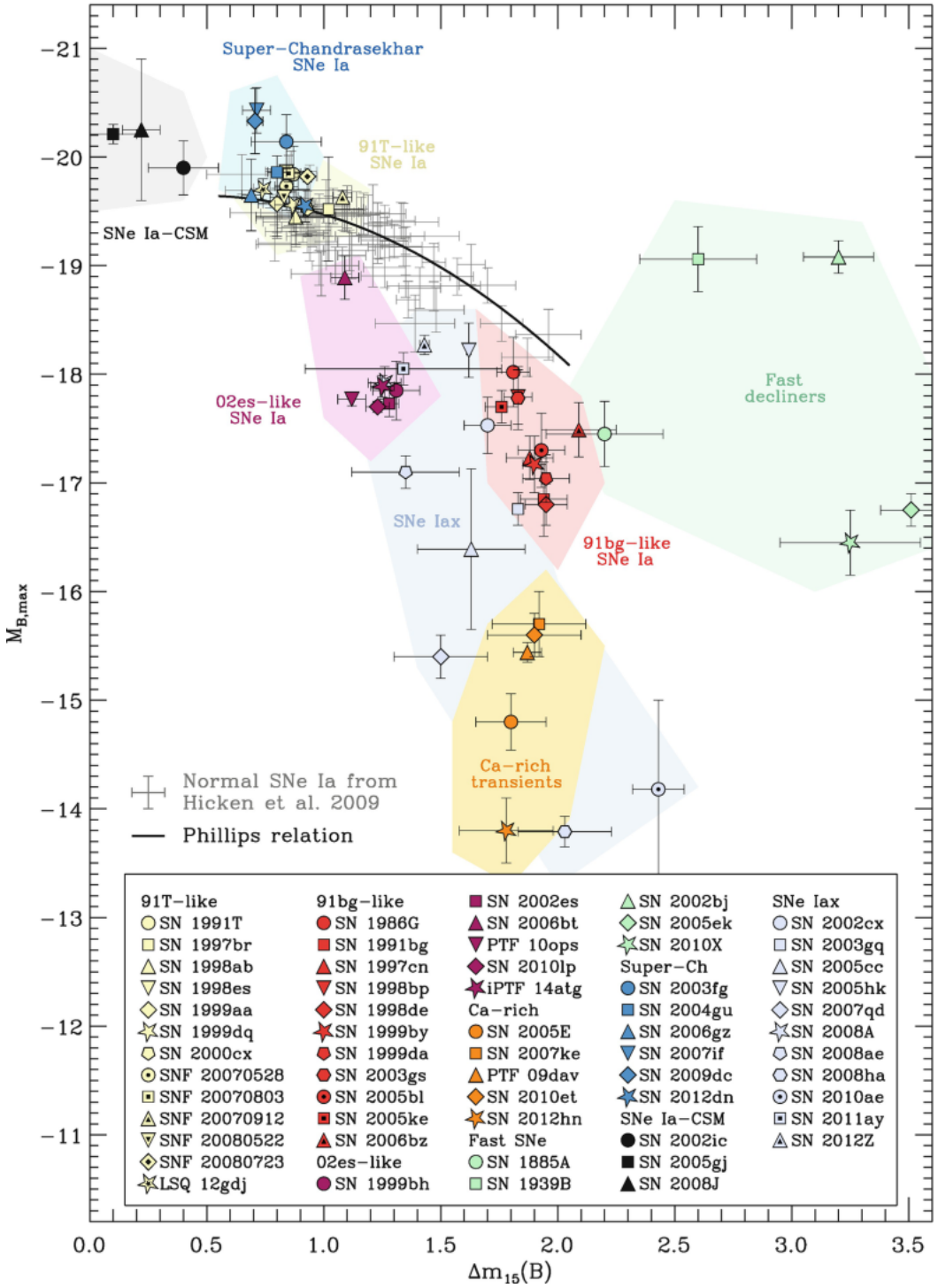

Figure 2.3: Peak B-band magnitude vs lightcurve decline rate highlighting the photometric differences observed over SNe Ia subclasses. [Taubenberger, 2017]

2.2.1 Progenitor Systems

In the SD model [Whelan and Iben, 1973] a non-degenerate star such as a main sequence star, a red giant, an asymtotic giant-branch star, or a helium star, plays the role of the binary companion. This star steadily transfers mass onto the WD until M_{Ch} is reached and a thermonuclear runaway occurs. Mass growth can occur through Roche-lobe overflow in which the companion star expands beyond its Roche-lobe and material from it flows onto the WD, or through stellar winds emitted by the non-degenerate star [Livio and Mazzali, 2018].

The SD model can help explain the observed homogeneity between SNe Ia light curves and spectra as it assumes the WD will explode very near M_{Ch}. On the other hand, it might explain the diversity observed over SNe Ia events since the SD model provides multiple progenitor channels that meet this mass requirement. The SD model has many weaknesses though. It needs delicate fine tuning of the parameters to actually lead to the thermonuclear explosion of the WD.

There exists a narrow range of accretion rates that can produce the required conditions for mass growth onto the WD leading to a SN Ia. This steady accretion ($\dot{M} \approx$ (a few) $\times 10^{-8} M_{\odot}$ yr^{-1} to $\dot{M} \approx$ (a few) $\times 10^{-7} M_{\odot}$ yr^{-1}) allows for stable nuclear burning of hydrogen to helium on the surface of the WD, and therefore mass buildup to M_{Ch} [Nomoto et al., 2007, Wolf et al., 2013, Hillman et al., 2016]. If the accretion rate is too high, the system may expand into a red giant configuration in which it experiences a common envelope phase, in which the envelope is eventually ejected, instead of becoming an SN Ia. A low accretion rate causes unstable burning which can lead to nova explosions. In this situation, accreted material is recurrently ejected therefore preventing the WD from reaching M_{Ch} [Livio and Mazzali, 2018].

From the observational side, searches for signatures of the companion star have so far been inconclusive. Observations of X-ray and radio emission from circumstellar material thought to arise in the SD model have so far led to non-detections, ruling out certain progenitors. Furthermore, the SD model has difficulty reproducing the observed SN Ia rate calculated through the DTD. Because of the constraints on the age of the companion star, this model can explain the 'prompt' part of the DTD, but not the 'delayed' part from SNe Ia observed in very old stellar systems [Jha et al., 2019].

The DD model in its simplest form involves two CO WDs of different masses in a binary system that merge due to emission of gravitational radiation [Webbink, 1984, Iben and Tutukov, 1984]. Their combined mass is assumed to exceed M_{Ch} leading to a SN Ia. In this scenario, the lighter

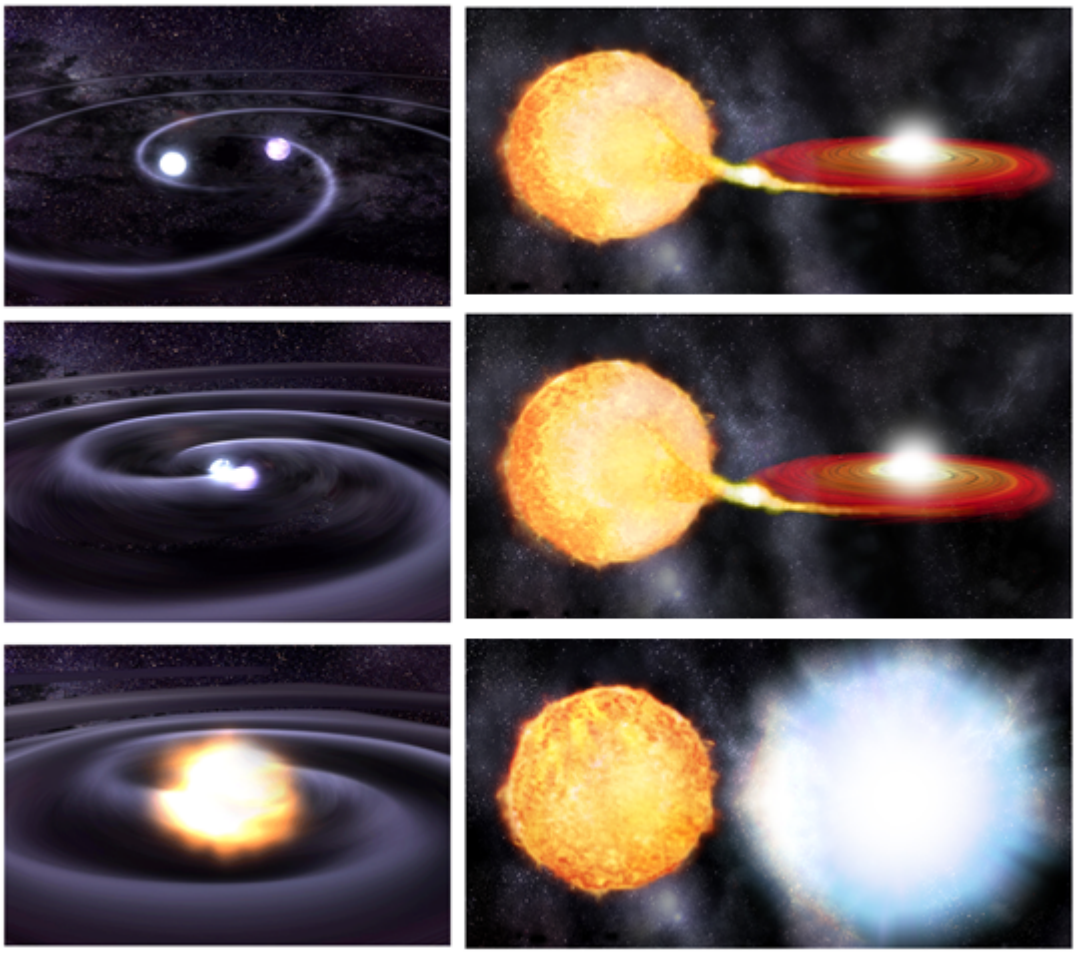

Figure 2.4: Graphic representing the single-degenerate (right) and double-degenerate (left) progenitor system models. Left: NASA/Tod Strohmayer (GSFC)/Dana Berry (Chandra X-Ray Observatory), Right: Discover magazine

of the two WDs (i.e. the WD with the larger radius, due to its degenerate nature) fills its Roche lobe which causes a dynamically unstable mass transfer during which a common envelope ensues. The mass donor becomes tidally disrupted, forming a massive disk around the primary WD, eventually resulting in a SN Ia explosion [Livio and Mazzali, 2018]. The DD model naturally explains the wide range of values observed in the DTD. For delay times longer than 1 Gyr, merging WDs have a DTD in clear agreement with observations due the orbit's decay from gravitational radiation [Heringer et al., 2017]. Short delay times behave like the production rate of WDs and are determined primarily by the lifetime of the less massive, WD producing, main sequence star [Pritchet et al., 2008]. Another strength of the DD model is that multiple population synthesis

studies have found that CO WD mergers are frequent enough to account for the Galactic SN Ia rates with certain assumptions regarding the common envelope evolution [Ruiter et al., 2009]. The non-detection of circumstellar hydrogen and a companion star also favors this model.

The DD model does have its weaknesses, a significant one being that it is theoretically difficult to produce a SN Ia explosion from a WD merger as it often leads to an accretion-induced collapse (AIC). Systems with a primary mass range of 1.0-1.1 $M_{\odot}$ and a secondary mass range of 0.5-0.7 $M_{\odot}$ tend to result in an AIC instead of a detonation of the primary WD according to [Sato et al., 2015]. This implies that the DD scenerio can only account for $\leq 9\%$ of the galactic rate. Lower-mass mergers are not predicted to produce enough ^{56}Ni to match observations, and it is unclear if they lead to thermonuclear explosions at all.

Both models have been studied in depth and include variations to the basic scenarios we have reviewed. The wide range of delay times and observed differences in the photometric and spectral properties of SNe Ia most likely implies that multiple progenitors channels can produce a thermonuclear explosion. Gamma-ray observations may be the key to constraining the unknown systems that lead to an SNe Ia.

2.2.2 Explosion Models

The mechanism by which a WD explodes is unclear, but hydrodynamic modelling of these events provides clues to how ignition is achieved. Observational constraints are used to discern the viability between models. The model must agree with the composition and velocity of the observed spectra and light curve; in particular it must be able to reproduce enough ^{56}Ni and a sufficient amount of high-velocity intermediate mass elements in the outer layers. The explosion mechanism must be able to account for the homogeneity of normal SNe Ia, thus it should not depend on the fine-tuning of parameters and initial conditions. The model must also correlate with the progenitor system in order to describe the variations between events based on the host stellar population [Hillebrandt and Niemeyer, 2000].

The first hydrodynamical simulation for an exploding WD [Arnett, 1969] assumed that combustion occurs as a detonation wave, or prompt detonation with a supersonic burning front. This model fails to produce enough intermediate mass elements to match observations as almost all of the C and O material is transformed into iron-peak elements. Thus, the burning front cannot be described by a pure detonation and must include a period of subsonic burning. The pure deflagration

model [Röpke and Hillebrandt, 2005] describes the propagation of the thermonuclear reaction in the form of a flame that starts out in the *deflagration mode*, meaning the burning front is mediated by microphysical processes and travels at subsonic speeds. This model has issues as it is difficult to actually gravitationally unbind the WD with a burning front that only travels at subsonic speeds. Delayed detonation combines the two models above so that it includes a transitional phase from subsonic to supersonic burning in the WD. Turbulent deflagrations have been found to undergo spontaneous transitions to detonations, or deflagration-detonation transitions (DDTs), so it is possible that this transition occurs in the later phases of the explosion, reproducing the large amounts of high-velocity intermediate mass elements observed in SN Ia spectra [Hillebrandt and Niemeyer, 2000].

Only certain details about the explosion mechanism can be derived from the available photometry and spectral properties, highlighting the need for gamma-ray observations of SNe Ia. Gamma-rays may reveal the types of burning fronts responsible for the observed velocities and nucleosynthesis products, answering the many unknowns about how a WD ignites and explodes to produce a SN Ia.

Chapter 3

SN Ia Rate Calculation

SNe rates are an incredibly important quantity for various fields in astrophysics. Understanding these rates is a necessary factor in describing the chemical evolution and metal enrichment of the Universe. SNe also play a key role in understanding the structure and composition of the interstellar medium (ISM), energy injection and feedback into galaxies, and the birth rate of compact objects [Leaman et al., 2011]. Because of their role in determining the expansion rate of the Universe and other fundamental constants, the rate of SNe Ia is particularly valuable. It can provide insight on the age distribution of SNe Ia progenitor systems, therefore providing limits on the timescales for the various progenitor scenarios. The fact that SNe Ia occur at different rates in different galaxy types has significant implications for the galactic environments that produce them, and can shed even more light on the physical mechanisms behind SNe Ia.

Several methods have been introduced to calculate the SNe rates in the local Universe. One approach is to determine the rate as a function of host galaxy properties, such as galaxy mass, luminosity, or color. Surveys have been used to identify trends between SNe Ia rates and host galaxy properties, such as the Nearby Supernova Factory (SNfactory) [Aldering et al., 2002], the Sloan Digital Sky Survey-II Supernova Survey [Frieman et al., 2008], the Palomar Transient Facility (PTF) [Law et al., 2009], and the All-Sky Automated Survey for Supernova (ASAS-SN) [Brown et al., 2019]. In particular, the Lick Observatory Supernova Search (LOSS) [Li et al., 2011a], identified the rate-size relation, or the correlation between host galaxy size (defined by mass or luminosity) and the rate of SNe Ia. This relation is what we use to determine the rate of SN Ia for each galaxy in our sample.

3.1 Control-Time Method

Measuring SNe rates as a function of galactic properties is, in theory, a straightforward procedure. Observatories monitor a sample of pre-selected galaxies (a "galaxy-targeted" survey) or a region of space out to a predefined volume (a "volumetric" survey) for SN events. A rate is then determined based on the number of SNe discovered and the "effective visibilty time" or "control time" and normalized to a galactic property, historically the B-band luminosity for galaxy-targeted surveys due to its use as a tracer of star formation. The control time is defined as the interval of time during which a possible SN would remain brighter than the limiting magnitude of the observation; in other words, how long a specific type of SN would remain observable by an instrument. Based on this, the control time is dependent on the adopted peak magnitude of the SN, its light-curve shape, and the limiting magnitude of the observation.

The control time $C_{i,j}$ is calculated for a single light-curve shape and luminosity at time t_i for the j^{th} galaxy as follows:

We define t_1, t_2,..., t_i,... as the epochs of observations, so $t_i - t_{i-1}$ is the time interval between observations $i-1$ and i. With a total of n observations for the j^{th} galaxy, the total control time tC_j is found as

$$tC_j = \sum_{i=1}^{n} \Delta t_i c_i, \quad \text{where} \qquad \Delta t_i = \begin{cases} C_{i,j} & \text{if } t_i - t_{i-1} \geq C_{i,j} \text{ or } i = 1 \\ t_i - t_{i-1} & \text{otherwise} \end{cases}. \tag{3.1}$$

Here c_i is a correction factor to account for the historical bias against SN discoveries in the nuclear regions of galaxies. The control time is normalized by galaxy luminosity (or mass), L_j, so that the normalized control time is

$$t_j = tC_j L_j \tag{3.2}$$

.

Then the final rate is given by

$$rate = \frac{N_{SN}}{\sum_{j=1}^{N_G} t_j} \tag{3.3}$$

where N_G is the number of galaxies in the sample and N_{SN} is the number of observed SNe [Cappellaro et al., 1997, Leaman et al., 2011].

Because of the observed diversity in SNe Ia peak luminosity and light curve evolution, assuming a standard light curve is an oversimplification that can lead to large uncertainties in the final rate calculation. To combat this, some studies have introduced a Gaussian scatter to the peak absolute magnitudes and/or stretched the light curve of the SN Ia based on its luminosity to better represent a diversity between events. [Li et al., 2011b] found this was not an appropriate representation, and instead derived a luminosity function for each SNe type. This luminosity function is slightly different from the standard definition in that it is composed of discrete components corresponding to individual peak magnitudes and light-curve shapes of SNe observed in a distance-limited sample.

Thus, the total control time t is calculated using the LF as,

$$t = \sum_{i=1}^{n} \Delta f_i t_i \tag{3.4}$$

where t_i is the total control time from the ith component in the LF and f_i is the fraction of the LF due to the ith component.

The total control time is normalized to a chosen parameter, such as the B-band luminosity, and the rate is again found using equation 3.2.

3.2 Rate-Size Relation

To calculate the rate for a sample of galaxies with different physical properties, one must group the galaxies based on some parameter that is correlated to the SNe rate. It was historically believed that galaxies of the same Hubble type or B-K color had comparable SNe rates, so galaxies are grouped according to these properties. The B-K color of a galaxy is correlated to its specific star formation rate (sSFR), or star formation rate per unit galaxy stellar mass. The B-band ($\lambda \approx 445$ nm) in general traces the younger, "bluer," more massive stellar population of a galaxy, while the K-band ($\lambda \approx 2190$ nm) traces its older, "redder," low mass stars. In essence, the B-K color defines how "blue" or "red" a particular galaxy is and furthermore gives clues to its stellar population ages and star formation rates. In their rate calculations using the control-time method, [Li et al., 2011a] determined that one parameter was not enough to accurately describe a galaxy's SNe rate, and that

the addition of a size parameter was needed. The galaxy size can be measured in either B or K band luminosity or stellar mass. This relationship between a galaxy's SNe rate and its size is the rate-size relation, and it is used to calculate the SN Ia rate for an individual galaxy. The relation is,

$$SNuB(L_B) = SNuB(L_{B0})\Big(\frac{L_B}{L_{B0}}\Big)^{RSS_B} \tag{3.5}$$

where $SNuB(L_{B0})$ is a fiducial rate based on the galaxy's B-K color, L_{B0} is the fiducial galaxy luminosity, and RSS_B is the rate-size slope (RSS) normalized by B-band luminosity. [Li et al., 2011a] found three separate RSS values based on normalization by the B-band, K-band, or stellar mass. We choose to calculate rates for individual galaxies based on the B-band normalization due to it being the best studied wavelength for SNe Ia. This is due to past detectors being most sensitive to this band. To determine the rate for a galaxy, its B-band luminosity, L_B is required. The final rate, $SNuB(L_B)$ is given in standard SNe rate units SNu, normalized to the B-band, or SNe 100 yrs^{-1} 10^{10} $L_{\odot}^{-1}$.

Chapter 4

Estimating Supernova Rates in the Local Universe

In this chapter, we calculate the SN Ia rate per galaxy using the rate-size relation (equation 3.5) for galaxies within the local Universe, which we define here as within 100 Mpc. We use data from the Galaxy List for the Advanced Detector Era (GLADE) catalog [Dálya et al., 2018] to determine the rate of SNe Ia for each galaxy. Using these rates, we then calculate the probability for one SN Ia to occur in each galaxy to then predict the number of SNe Ia we expect over ten years for galaxies within the local Universe.

4.1 GLADE Catalog

The Galaxy List for the Advanced Detector Era (GLADE) catalog is a full-sky catalog created primarily to assist in identifying electromagnetic counterparts to transient gravitational wave events. It was constructed by cross-matching and combining data from five separate (but not independent) astronomical catalogs: the GWGC [White et al., 2011], the HyperLEDA catalogue [Makarov et al., 2014], the 2 Micron All-Sky Survey Extended Source Catalog (2MASS XSC) [Skrutskie et al., 2006], the 2MASS Photometric Redshift Catalog (2MPZ) [Bilicki et al., 2014], and the Sloan Digital Sky Survey quasar catalogue from the 12th data release (SDSS-DR12Q) [Pâris et al., 2017]. GLADE includes a total of 3,262,881 objects, 2,965,718 of which are galaxies. In terms of cumulative

B luminosity, it is complete up to $d_L = 37^{+3}_{-4}$ Mpc. Furthermore, it contains all of the bright galaxies giving half of the total B luminosity up to $d_L = 91$ Mpc, giving it ∼61 percent completeness for d_L within 100 Mpc. Figure 4.1 shows the distribution of GLADE galaxies within 100 Mpc as an Aitoff projection. Galaxies are plotted in galactic coordinates and color coded based on their luminosity distance. The location of the galactic plane is visible from the lack of observations due to dust and gas obscuring objects behind it.

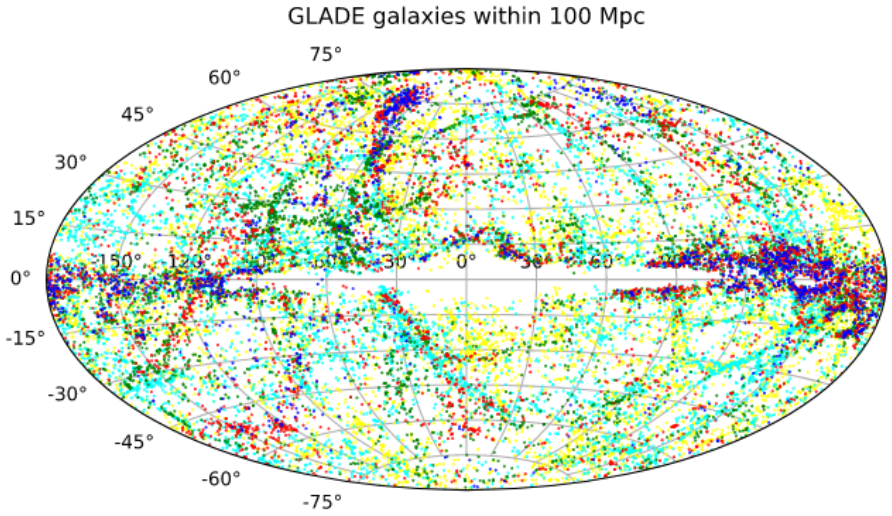

Figure 4.1: Aitoff projection of GLADE galaxies within 100 Mpc plotted in galactic coordinates, with 31,892 objects in total. Galaxies are color coded based on their distance bins. Blue: 0-20 Mpc, red: 20-40 Mpc, green: 40-60 Mpc, cyan: 60-80 Mpc, and yellow: 80-100 Mpc.

It is evident from figure 4.1 that galaxies are not evenly distributed in each distance bin, highlighting the need to obtain accurate rates within the local Universe based on the actual distribution of galaxies and their properties. Figure 4.2 shows the distribution of GLADE galaxies within 40 Mpc. The inhomogeneity in galaxy distribution becomes even more apparent within 40 Mpc, where galaxies are found in clusters in certain portions of the sky.

As stated previously, the GLADE catalog contains 2,965,718 galaxies in total. 62,379 galaxies are within 100 Mpc, out of which 57,411 have measured apparent B-band magnitude and 31,990 have apparent K-band magnitude. This leaves a total of 31,892 galaxies within 100 Mpc that have data required to calculate a SNe rate. Rates for almost half of our sample galaxies cannot be calculated because they do not have a measured K-band magnitude. To see how this might affect our total rates, we graph the distribution of absolute B and K magnitudes in figure 4.3.

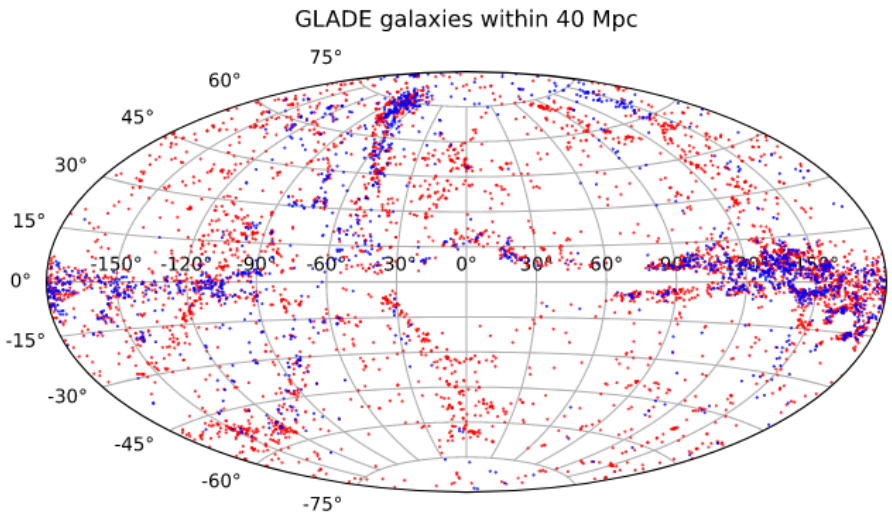

Figure 4.2: Aitoff projection of GLADE galaxies within 40 Mpc plotted in galactic coordinates, with 5,909 galaxies in total. Color code is the same as figure 4.1.

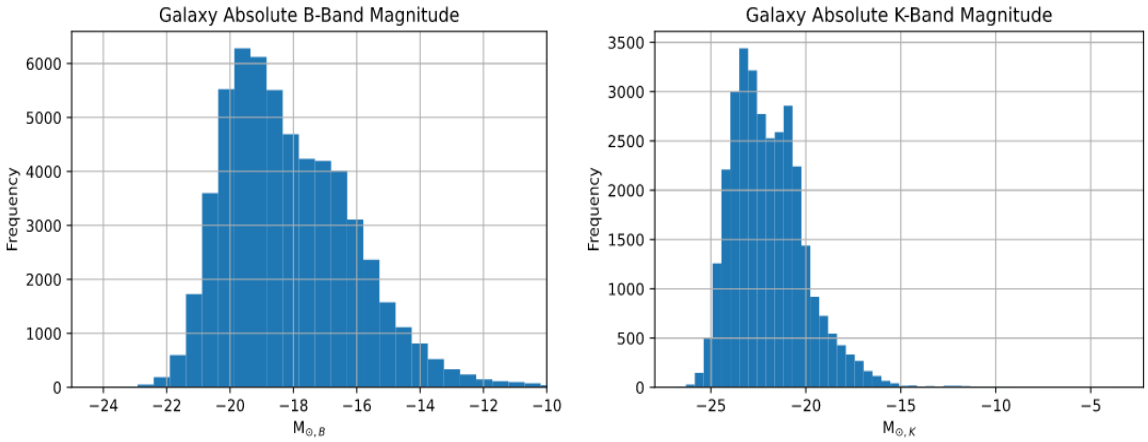

Figure 4.3: Distribution of absolute B-band (left) and K-band (right) magnitudes for GLADE galaxies within 100 Mpc.

Average B-band magnitudes for spirals range from -17 to -23, while ellipticals range from -17 to -22. Irregular galaxies in general have B-band magnitudes $\leq$-17 [Cimatti et al., 2019]. According to figure 4.3, many of the galaxies within 100 Mpc have absolute B-band magnitudes typical for an irregular galaxy.Thus, we attribute a majority of the data loss to lack of K-band measurements of irregular galaxies. This has a minor affect on our determination of the local rate because according to [Li et al., 2011a], irregular Hubble types have typical SNe Ia rates in $SNuB$ equal to $\approx$0.

4.2 Calculating SN Ia rate per galaxy

Equation 3.5 is used to calculate the rate of SNe Ia for each galaxy in the catalog that meets the required criteria. The apparent B magnitude, m_B, apparent K magnitude, m_K, and luminosity distance, d_L, (in Mpc) are obtained from GLADE.

To use the rate-size relation, the B-band luminosity must be calculated for each galaxy. First, m_B is converted to absolute B magnitude, M_B, using the equation:

$$M_B = m_B - 5log\frac{d(pc)}{10pc} \tag{4.1}$$

.

The luminosity of the galaxy in the B-band with units of $L_\odot$ is found from the equation:

$$L_B = 10^{\frac{M_{B\odot} - M_B}{2.5}} \tag{4.2}$$

where $M_{B\odot} = 5.48$ is the absolute magnitude of the sun measured in the B-band.

The B-K color of each galaxy is needed to determine the appropriate fiducial galaxy SN rate and is calculated directly from the apparent B and K magnitudes. These values are divided according to Table 4.1 which shows the B-K color ranges for each galaxy group, its corresponding SNuB or SN rate value, in units of SNe 100 yrs^{-}1 10^{10} $L_{\odot,B}$ and the number of SNe Ia used to calculate the fiducial rate. (Note B-K upper bound is open, i.e. [2.3, 2.8), [2.8, 3.1), etc.) Figure 4.4 displays the distribution of B-K colors in our galaxy sample. A large dip is apparent around ≈4 due to the lack of K band data. Our sample favors bluer, later type galaxies with B-K <4.

B-K	SNuB(L_{B0})	Number of SN Ia used
> 2.3	$0.158^{+0.051}_{-0.040}$ (0.043)	15.6
2.3-2.8	$0.152^{+0.039}_{-0.032}$ (0.030)	22.6
2.8-3.1	$0.231^{0.043}_{-0.036}$ (0.054)	39.8
3.1-3.4	$0.248^{+0.040}_{-0.035}$ (0.043)	50.2
3.4-3.7	$0.260^{+0.041}_{-0.035}$ (0.047)	53.6
3.7-4.0	$0.250^{+0.043}_{-0.037}$ (0.052)	46.0
>4.0	$0.305^{+0.054}_{-0.046}$ (0.056)	43.0

Table 4.1: SN Ia rates in fiducial galaxies adapted from Table 5 of [Li et al., 2011a]

For the chosen B-band normalization, the fiducial galaxy luminosity is given as $L_{B0} = 2 \times 10^{10}$ $L_\odot$ with a rate-size slope $RSS_B = -0.25 \pm 0.15$. With all of these ingredients, the rate of

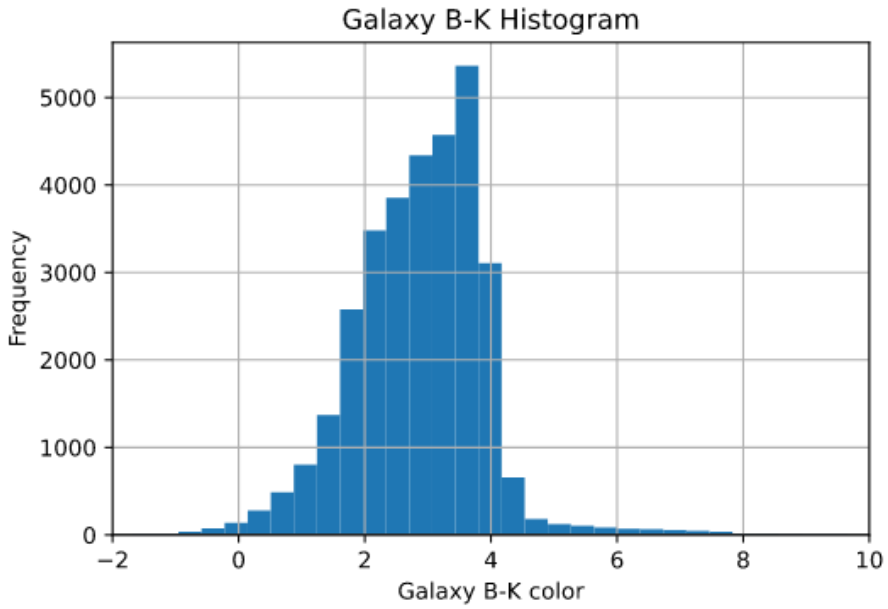

Figure 4.4: B-K color distribution for GLADE galaxies within 100 Mpc.

SN Ia can be calculated for each galaxy using Equation 3.5.

Galaxy Name	d_L (Mpc)	m_B	M_B	m_K	L_B ($\times 10^{10}$ $L_\odot$)	B-K	SNuB (L_{B0})	SNuB (L_B)	SNe 100 yrs^{-1}
NGC0055	2.188	7.50	-19.20	6.562	0.745	0.938	0.158	0.202	0.151
NGC4548	17.701	10.85	-20.39	7.368	2.228	3.482	0.260	0.253	0.564
NGC6503	4.285	10.280	-17.88	7.388	0.221	2.898	0.231	0.401	0.088
NGC4808	55.23	11.928	-21.783	9.153	8.04	2.775	0.152	0.107	0.863
NGC4387	17.947	12.82	-18.45	9.234	0.373	3.586	0.260	0.396	0.148
NGC4144	6.668	11.20	-17.92	9.922	0.229	1.278	0.158	0.272	0.062
NGC4328	8.083	14.08	-15.46	11.732	0.024	2.357	0.152	0.461	0.011
NGC1291	10.978	10.431	-19.77	5.852	1.261	4.579	0.305	0.342	0.432
NGC7793	3.945	9.52	-18.46	7.250	0.377	2.270	0.158	0.239	0.090
NGC4442	15.276	11.29	-19.63	7.381	1.106	3.910	0.250	0.290	0.321

Table 4.2: Galaxy properties and final rate value for select galaxies

Table 4.2 shows a sample of the data used to calculate the rate for select galaxies in the GLADE catalog and the final rate for each galaxy, given in SNuB (SNe 100 yrs^{-1} 10^10 $L^{-1}_{\odot,B}$). Column 1 lists the galaxy name as given in the HyperLEDA catalog. Column 2 gives the luminosity distance, d_L, in Mpc. Columns 3 and 5 give the apparent B and K magnitudes, respectively. The absolute B-band magnitude is given in column 4 and is calculated using equation 4.1. Equation 4.2 is used to calculate the B-band luminosity in column 6, with units of 10^{10} $L_\odot$. Column 7 lists the difference between the apparent B and K magnitude. Column 8 gives the fiducial SN rate according to table 4.1. Column 9 gives the galactic SN rate in SNuB. Column 10 lists the SN rate per century

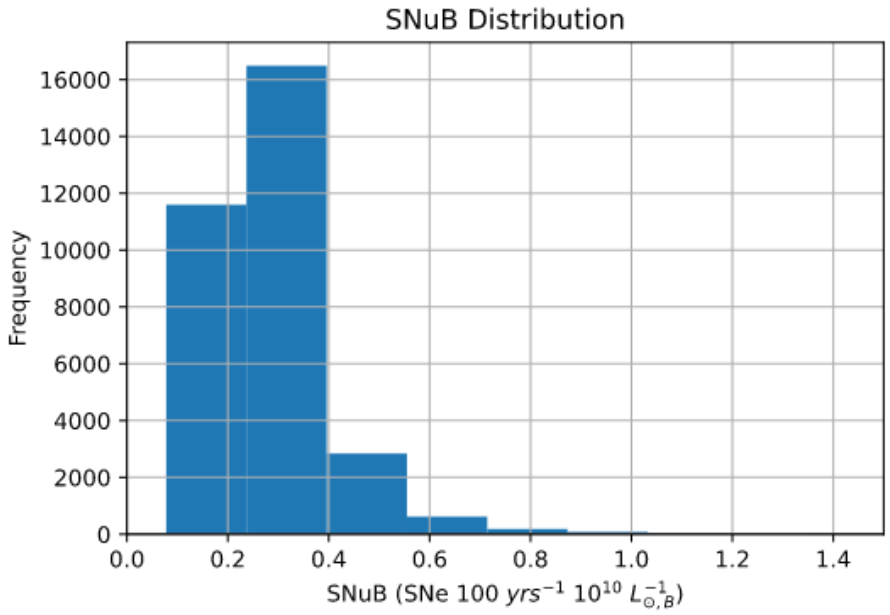

Figure 4.5: Distribution of galactic SN Ia rates in units of SNuB (standard SN rate unit normalized to B-band luminosity.)

by dividing the measured galaxy luminosity L_B by the normalization factor 10^{10} $L_{\odot,B}$. Figure 4.5 shows the distribution of galactic SNe Ia rates in the standard units of SNu normalized to the B-band (SNe 100 $yrs^{-}1$ 10^{10} $L_{\odot}^{-1}$). It is shown that the bulk of galaxies within 100 Mpc have a rate between ∼0.2-0.4 SNuB. Although it is useful to view the rates normalized to the galaxy luminosity, our goal is to predict the number of SNe Ia occurrences over some time period, specifically the average duration of a gamma-ray detector. Therefore we also determine the rate in units of events per century. This is represented in figure 4.6.

4.3 Simulating SN Occurrences in the Local Universe

With the SN rate calculated for each galaxy, it is now possible to estimate the expected number of SN events over some time period. For the purpose of this work, we estimate the number of SNe Ia over ten years, or the average duration of a gamma-ray observatory.

First, the calculated rate per century for each galaxy is converted to a rate per decade. This value becomes the probability of a SN Ia event under the assumption that each galaxy will only have one event in this time period. This is an appropriate assumption based on observations. Whether

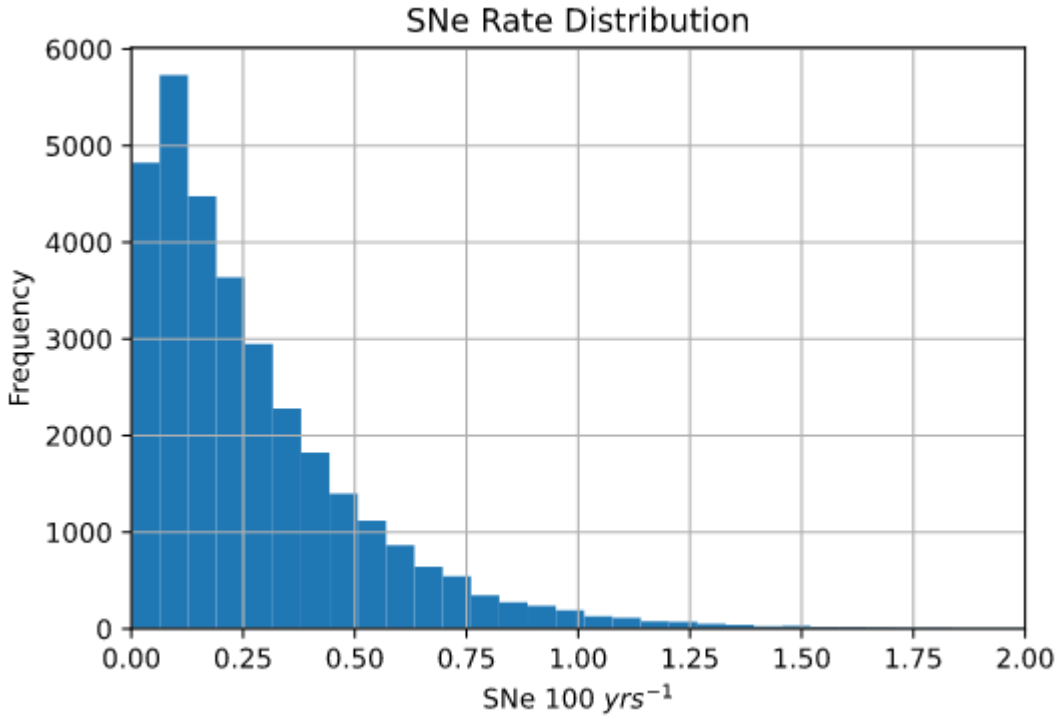

Figure 4.6: SN Ia rate per century.

or not a specific galaxy will have an SN Ia event over a span of 10 years is determined by comparing the calculated probability to a random number generator. The idea is as follows: A random number between 0 and 1 is generated for each galaxy in the sample. If the generated number is less than the calculated probability, that galaxy is flagged true for a SN Ia event. Values that are greater than the probability indicate that no SN event occurred. Using our probability and the random number generator, we estimate the total number of SNe Ia per decade. We present the results of this method in the next section.

Chapter 5

Results and Comparisons

In the previous section, we used photometric data and equation 3.5 to derive the SN Ia rate for each galaxy in our sample. Furthermore, we applied these rates to determine the probability of one SN Ia event in each galaxy over a time period of 10 yrs. With these probabilities, we estimated the number of SN Ia events that are expected to occur within the local Universe. In this section, we present the results of our simulation.

5.1 Estimating number of SNe Ia

From a sample of 31,982 galaxies within the local Universe, we find an average of ∼890 SNe Ia are expected to occur every decade within the local universe (<100 Mpc). This is the mean value of 20 separate renditions of the probability versus random number generator simulation. The actual count is expected to be slightly higher due to the loss of galaxies in the sample from lack of K-band data. Note that this estimate does not represent the number of events that will be observable as they are limited by factors such as the limiting magnitude of the detector and extinction. Instead, this is a prediction of the number of SN Ia events expected to occur based on the physical properties and distribution of galaxies in the local universe. However, we choose to simulate events within the nearby Universe so detectors are less affected by distance related consequences such as extinction. SNe Ia are also extremely bright objects and so are less likely to be missed locally.

These results are comparable to those of [Horiuchi and Beacom, 2010] who find an expected local rate of ≈100 SNe Ia per year within 100 Mpc based on SN catalog data and a cosmic SN Ia rate

derived using the delay-time distribution. [Frohmaier et al., 2019] also derived a volumetric rate for the local universe of $\approx 2.43 \times 10^{-5}$ SNe yr^{-1} Mpc$^{-}3$, or 100.5 per year within 100 Mpc using a sample of SNe Ia from PTF.

5.2 Mapping Simulated SNe Ia Events

To investigate any trends within the our local SNe rates based on distance, we plot the distribution of galaxy distances to compare to the frequency of simulated SNe Ia binned by galaxy distance for four outcomes of the simulation. Logically, more SNe Ia are expected to occur where there is a larger number of galaxies, despite the SNe Ia rates' dependence on galaxy properties. Nevertheless, identifying specific locations or distances where more events are expected and that already have cataloged galaxy data can provide useful information for prospective gamma-ray detectors.

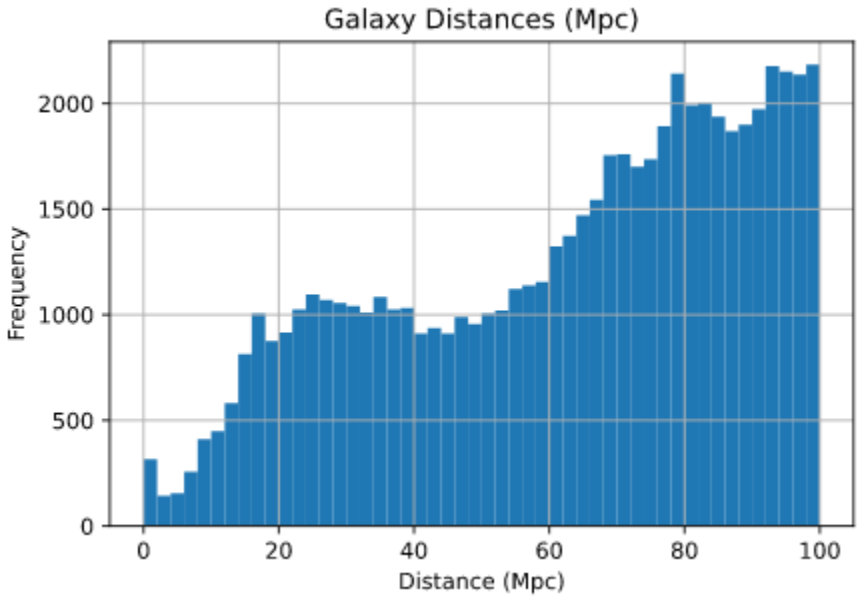

Figure 5.1: Galaxy distance histogram for GLADE galaxies within 100 Mpc.

Figure 5.1 shows the distribution of GLADE galaxy distances for galaxies within 100 Mpc. A "bump" in the number of galaxies is found between 20 to 40 Mpc and again around 60 to 80 Mpc. We expect more simulated SN Ia events between these ranges, from the increased number of galaxies. To examine this, we plot the frequency of simulated SNe Ia distances within 100 Mpc in figure 5.2.

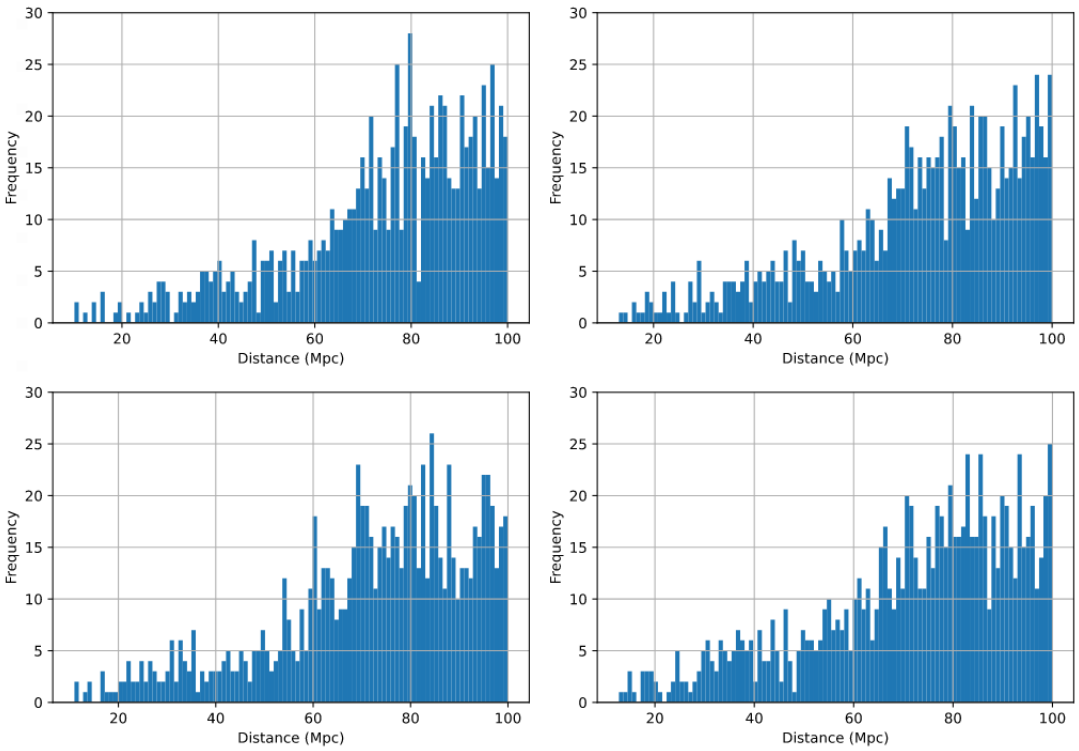

Figure 5.2: SNe Ia event distance histogram for four runs. Top left: 846 SNe Ia, Top right: 868 SNe Ia, Bottom left: 905 SNe Ia, Bottom right: 942 SNe Ia.

Clockwise beginning from top right, Figure 5.2 shows the distribution of 846, 868, 942, and 905 SNe Ia from four individual outcomes of the simulation. This represents the lower to upper range of the simulation. We do find a corresponding increased frequency of events within 20 to 40 Mpc and 60 to 80 Mpc compared to the distances between 40 to 60 Mpc and 80 to 100 Mpc. The frequency of events within these latter ranges tend to plateau unlike the former in which the number of events rises as distance increases.

To investigate the locations where more events are expected over a time span of ten years, we also map the simulated SNe Ia as an Aitoff projection in galactic coordinates in figures 5.3 and 5.4. Figure 5.3 shows the locations of simulated SNe Ia within 100 Mpc color coded by distance where blue represents events between 0-20 Mpc, red is between 20-40 Mpc, green is 40-60 Mpc, cyan is 60-80 Mpc, and yellow is 80-100 Mpc. We map four individual outcomes of the simulation, representing the low, middle, and high end of the total range of the number of simulated SNe Ia. Events within 100 Mpc are in general distributed uniformly across the sky, with some areas exhibiting a slightly higher density corresponding to a higher density of host galaxies. When we focus on very nearby

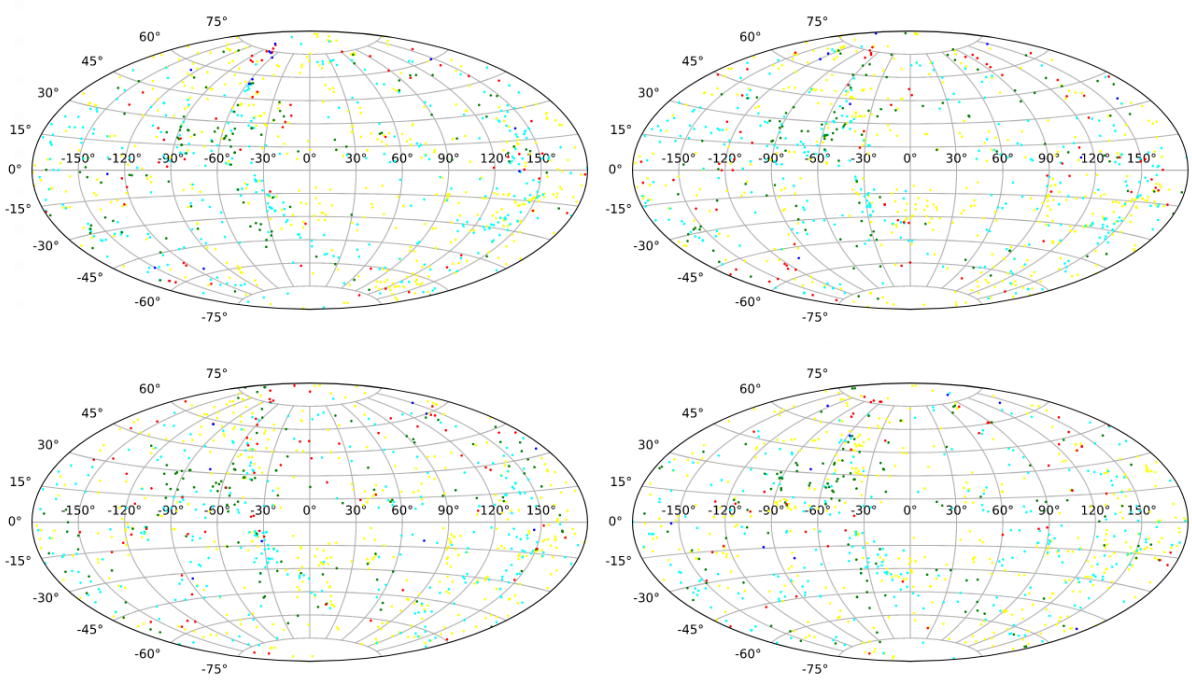

Figure 5.3: Aitoff projection of simulated SNe Ia plotted in galactic coordinates. Galaxies are color coded based on their distance bins. Blue: 0-20 Mpc, red: 20-40 Mpc, green: 40-60 Mpc, cyan: 60-80 Mpc, and yellow: 80-100 Mpc. Top left: 937 SNe Ia, Top right: 904 SNe Ia, Bottom left: 877 SNe Ia, Bottom right: 856 SNe Ia.

events within 0 to 40 Mpc, the uniformity of the distribution of SNe Ia disappears, as shown in figure 5.4. In this figure, it is evident that certain areas of the sky are expected to have more SN Ia events within 40 Mpc in ten years based on the distribution of galaxies.

5.3 Rates as a Function of Distance

Oftentimes in rate calculations, it is assumed that if galaxies are equally distributed within some volume, the SN Ia rate can be described in general as a function of distance with form d^3. (i.e. as distance increases, the number of galaxies enclosed will be proportional to the volume). In reality, the Universe is not so simple. Not only are galaxies distributed unevenly within the local universe, their properties vary over a wide range of masses, ages, types, etc. We have estimated how many events we expect on average over ten years within the local Universe and found a rate of approximately 89 SNe Ia per decade. Now, we investigate how well our number of simulated events calculated based on the physical properties of galaxies in the local universe follows this general

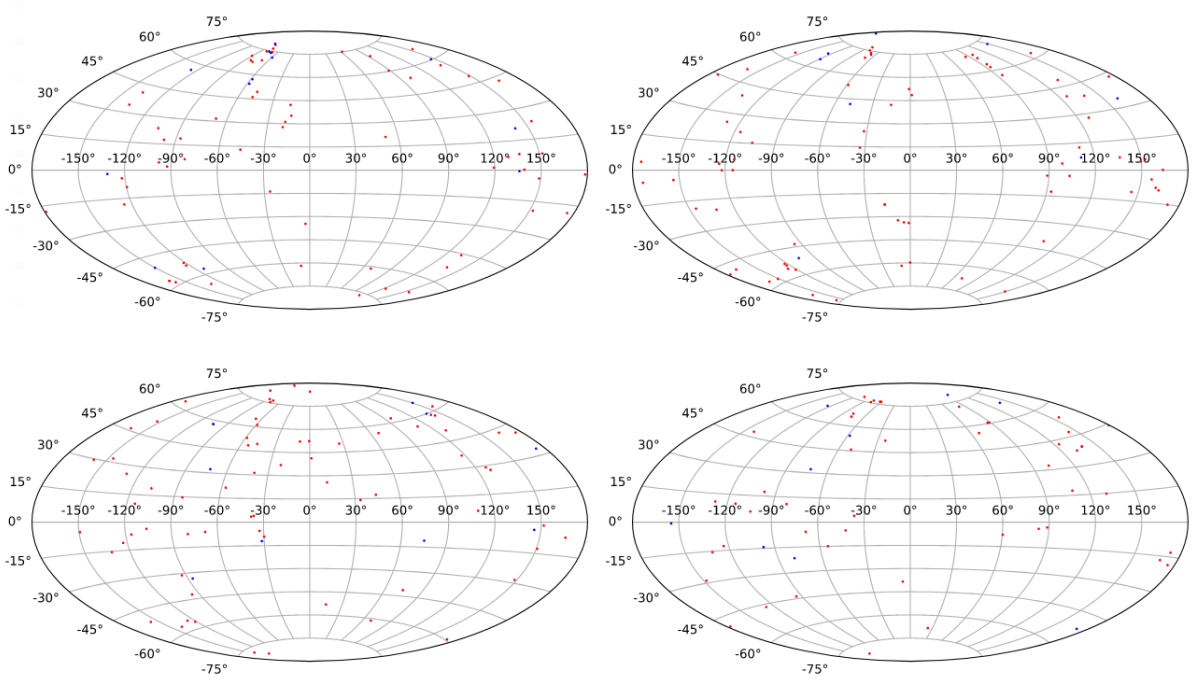

Figure 5.4: Same as figure 5.3, with only events within 40 Mpc plotted.

volumetric trend.

First, the cumulative frequency for four simulation outcomes are shown in figure 5.5. Little variation is found between the different outcomes in terms of the overall increase in SNe Ia as distance increases. To better visual the overall trend, the cumulative frequency per distance bin data is replotted in figure 5.6 as blue dots. The red line is the function ad^3 where a is a scale factor to fit to the data.

In figure 5.6, we find that the frequency overall fits the expected trend of d^3 with the biggest variations coming from the total number of simulated events for the separate runs. The low count of SNe Ia (846 events) initially follows the trendline until approximately 50 Mpc where it tends to stay lower than the expected values. The high end of the simulated SNe Ia (942 events) shows an excess of events compared to the trendline until approximately 90 Mpc. The incompleteness of the GLADE catalog at distances > 90 Mpc is apparent in all of the plots where the red distance function overtakes the blue cumulative frequency data. From figure 5.2, we expect a higher number of events between 20 to 40 Mpc and 60 to 80 Mpc. This is also found in figure 5.6 where the blue data points again show a "bump" in frequency in these ranges compared to the red trend line.

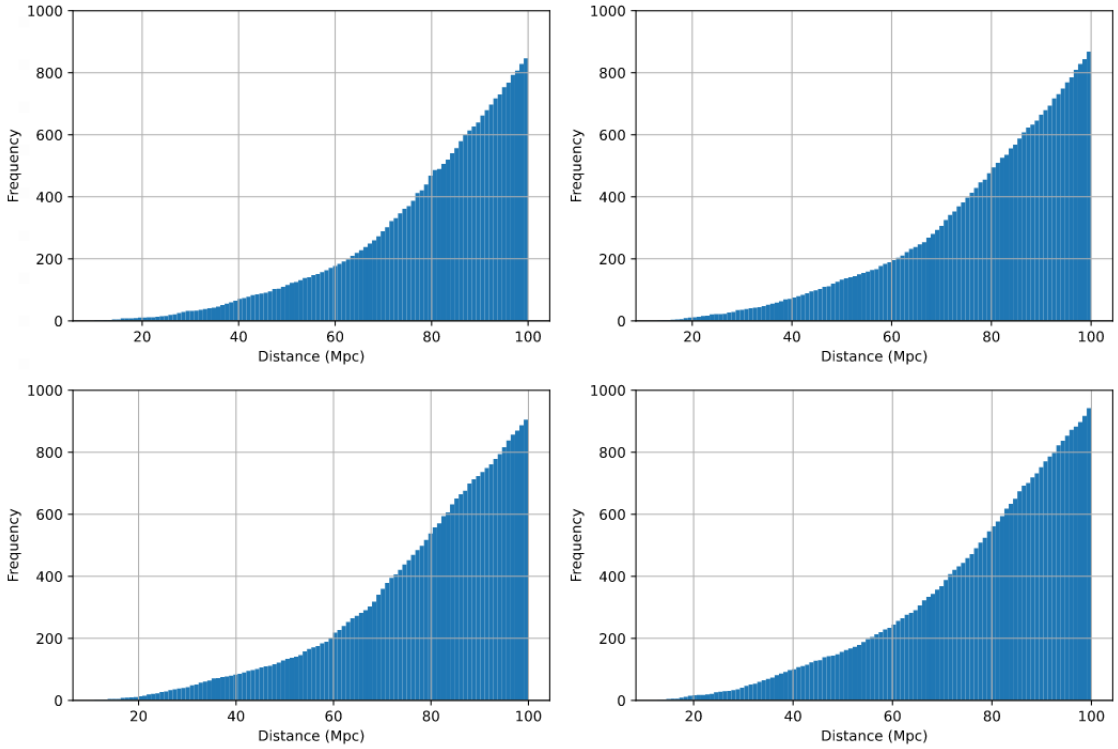

Figure 5.5: Cumulative frequency of SNe Ia events as a function of distance for four runs-Top left: 846 SNe Ia, Top right: 868 SNe Ia, Bottom left: 905 SNe Ia, Bottom right: 942 SNe Ia.

Figure 5.7 shows the cumulative frequency outcome of two simulations between 0 to 40 Mpc. The excess of SNe Ia is much more apparent between 20 to 40 Mpc when we focus on smaller distances. This is exciting news for prospective gamma-ray detectors as a larger than expected number of SNe Ia are predicted to occur within 40 Mpc. Nearby events are more easily observed as they are less affected by extinction and other distance related consequences. Prospective gamma-ray detectors can expect a large amount of SNe Ia within the local Universe compared to historical observations. Furthermore, we show that the number of events scales with volume, implying an increased number of events at larger distances, supplying much needed data at high redshifts. With gamma-ray observations of SNe Ia, many of the unknowns regarding these events will be revealed.

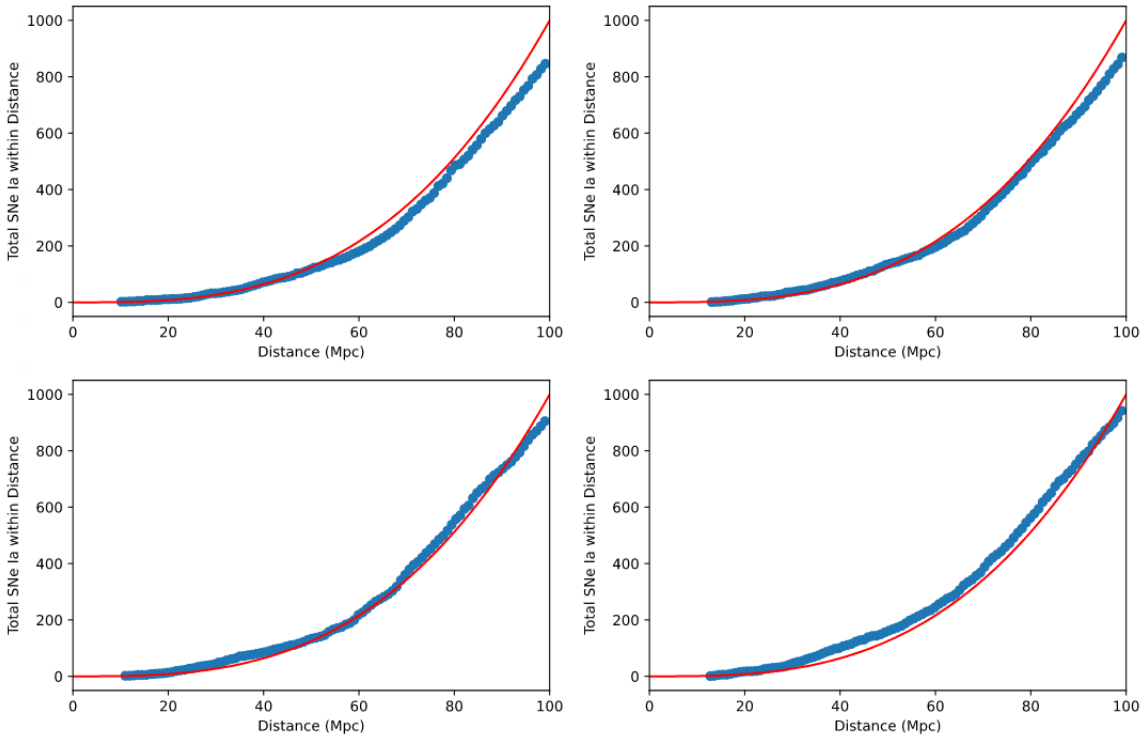

Figure 5.6: Blue dots represent the cumulative frequency of SNe Ia events as a function of distance for four runs-Top left: 846 SNe Ia, Top right: 868 SNe Ia, Bottom left: 905 SNe Ia, Bottom right: 942 SNe Ia. The red line is the function ad^3 where a=0.001 is a scale factor to fit to the data.

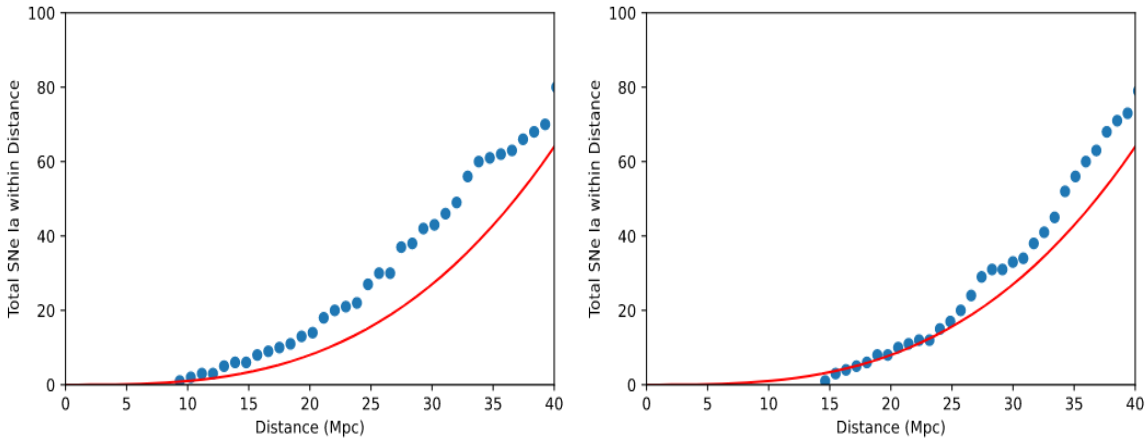

Figure 5.7: Simulated cumulative frequency-same as figure 5.6 for events within 40 Mpc.

Chapter 6

Conclusion

In this work, we investigate the rate of SNe Ia in the local Universe by predicting SNe Ia events based the distribution of cataloged galaxies within 100 Mpc.

In Chapter 3, we discuss the rate-size relation and its derivation from the control-time method applied to LOSS observations. In Chapter 4, we review our galaxy sample, the GLADE catalog, and the data required from it to calculate the rate for each galaxy. We obtain the apparent magnitude in the B-band and K-band and luminosity distance from GLADE and are left with 31,982 galaxies to calculate SNe Ia rates. We also apply the rate-size relation to individual galaxies to determine their SN Ia rate based on their B-band luminosity. Using these rates, we determine the probability of a SN Ia event over the span of ten years for each galaxy and compare it to a randomly generated number to simulate if one has occurred or not.

Chapter 5 reports the results of our simulation. We expect an average of 89 SNe Ia per decade within 100 Mpc. Plotting the simulated SNe Ia over distance shows an excess of events between 20 to 40 Mpc, providing a wealth of data for gamma-ray detectors dedicated to investigating the inner mechanisms of thermonuclear SNe. We map the locations where more SNe Ia are expected on average and find an overall uniform distribution within 100 Mpc. When we focus on very nearby events, we find more clumping of events corresponding to the distribution of galaxies within 40 Mpc. These trends are useful to prospective gamma ray missions to recognize certain distances and areas that are expected to have a higher density of events.

Our rates are modeled as a function of distance with form ad^3 where a is a scale factor included to fit to our data. We find it is possible to reproduce published rates by using the physical

properties of a catalog of nearby galaxies and the rate-size relation of [Li et al., 2011a]. Our rate is a lower limit based on the number of galaxies cut from our sample due to lack of K-band measurements, but we argue that a majority of the galaxies not included are irregular galaxies based on their B-band absolute magnitudes. This Hubble type is reported to have rates ≈ 0 SnuB so would not have had a major effect on our rate calculation.

Prospective gamma-ray missions focusing on the MeV nuclear gamma-ray regime will be able to investigate the main issues regarding thermonuclear SNe: the unknown progenitor systems and explosion mechanisms that lead to a SNe Ia. Based on our local rate calculation, enough events are expected to occur within a decade to provide the data needed to answer these remaining questions.

Bibliography

[Aldering et al., 2002] Aldering, G., Adam, G., Antilogus, P., Astier, P., Bacon, R., Bongard, S., Bonnaud, C., Copin, Y., Hardin, D., Henault, F., Howell, D. A., Lemonnier, J.-P., Levy, J.-M., Loken, S. C., Nugent, P. E., Pain, R., Pecontal, A., Pecontal, E., Perlmutter, S., Quimby, R. M., Schahmaneche, K., Smadja, G., and Wood-Vasey, W. M. (2002). Overview of the Nearby Supernova Factory. In Tyson, J. A. and Wolff, S., editors, *Survey and Other Telescope Technologies and Discoveries*, volume 4836 of *Society of Photo-Optical Instrumentation Engineers (SPIE) Conference Series*, pages 61–72.

[Arnett, 1969] Arnett, W. D. (1969). A Possible Model of Supernovae: Detonation of ^{12}C. , 5(2):180–212.

[Arnett, 1982] Arnett, W. D. (1982). Type I supernovae. I - Analytic solutions for the early part of the light curve. , 253:785–797.

[Bilicki et al., 2014] Bilicki, M., Jarrett, T. H., Peacock, J. A., Cluver, M. E., and Steward, L. (2014). Two Micron All Sky Survey Photometric Redshift Catalog: A Comprehensive Three-dimensional Census of the Whole Sky. , 210(1):9.

[Brown et al., 2019] Brown, J. S., Stanek, K. Z., Holoien, T. W. S., Kochanek, C. S., Shappee, B. J., Prieto, J. L., Dong, S., Chen, P., Thompson, T. A., Beacom, J. F., Stritzinger, M. D., Bersier, D., and Brimacombe, J. (2019). The relative specific Type Ia supernovae rate from three years of ASAS-SN. , 484(3):3785–3796.

[Cappellaro et al., 1997] Cappellaro, E., Turatto, M., Tsvetkov, D. Y., Bartunov, O. S., Pollas, C., Evans, R., and Hamuy, M. (1997). The rate of supernovae from the combined sample of five searches. , 322:431–441.

[Cimatti et al., 2019] Cimatti, A., Fraternali, F., and Nipoti, C. (2019). Introduction to Galaxy Formation and Evolution. From Primordial Gas to Present-Day Galaxies. *arXiv e-prints*, page arXiv:1912.06216.

[Dálya et al., 2018] Dálya, G., Galgóczi, G., Dobos, L., Frei, Z., Heng, I. S., Macas, R., Messenger, C., Raffai, P., and de Souza, R. S. (2018). GLADE: A galaxy catalogue for multimessenger searches in the advanced gravitational-wave detector era. , 479(2):2374–2381.

[Elias et al., 1985] Elias, J. H., Matthews, K., Neugebauer, G., and Persson, S. E. (1985). Type I supernovae in the infrared and their use as distance indicators. , 296:379–389.

[Filippenko, 1997] Filippenko, A. V. (1997). Optical Spectra of Supernovae. , 35:309–355.

[Frieman et al., 2008] Frieman, J. A., Bassett, B., Becker, A., Choi, C., Cinabro, D., DeJongh, F., Depoy, D. L., Dilday, B., Doi, M., Garnavich, P. M., Hogan, C. J., Holtzman, J., Im, M., Jha, S., Kessler, R., Konishi, K., Lampeitl, H., Marriner, J., Marshall, J. L., McGinnis, D., Miknaitis, G.,

Nichol, R. C., Prieto, J. L., Riess, A. G., Richmond, M. W., Romani, R., Sako, M., Schneider, D. P., Smith, M., Takanashi, N., Tokita, K., van der Heyden, K., Yasuda, N., Zheng, C., Adelman-McCarthy, J., Annis, J., Assef, R. J., Barentine, J., Bender, R., Blandford, R. D., Boroski, W. N., Bremer, M., Brewington, H., Collins, C. A., Crotts, A., Dembicky, J., Eastman, J., Edge, A., Edmondson, E., Elson, E., Eyler, M. E., Filippenko, A. V., Foley, R. J., Frank, S., Goobar, A., Gueth, T., Gunn, J. E., Harvanek, M., Hopp, U., Ihara, Y., Ivezić, Ž., Kahn, S., Kaplan, J., Kent, S., Ketzeback, W., Kleinman, S. J., Kollatschny, W., Kron, R. G., Krzesiński, J., Lamenti, D., Leloudas, G., Lin, H., Long, D. C., Lucey, J., Lupton, R. H., Malanushenko, E., Malanushenko, V., McMillan, R. J., Mendez, J., Morgan, C. W., Morokuma, T., Nitta, A., Ostman, L., Pan, K., Rockosi, C. M., Romer, A. K., Ruiz-Lapuente, P., Saurage, G., Schlesinger, K., Snedden, S. A., Sollerman, J., Stoughton, C., Stritzinger, M., Subba Rao, M., Tucker, D., Vaisanen, P., Watson, L. C., Watters, S., Wheeler, J. C., Yanny, B., and York, D. (2008). The Sloan Digital Sky Survey-II Supernova Survey: Technical Summary. , 135(1):338–347.

[Frohmaier et al., 2019] Frohmaier, C., Sullivan, M., Nugent, P. E., Smith, M., Dimitriadis, G., Bloom, J. S., Cenko, S. B., Kasliwal, M. M., Kulkarni, S. R., Maguire, K., Ofek, E. O., Poznanski, D., and Quimby, R. M. (2019). The volumetric rate of normal type Ia supernovae in the local Universe discovered by the Palomar Transient Factory. , 486(2):2308–2320.

[Gal-Yam, 2017] Gal-Yam, A. (2017). *Observational and Physical Classification of Supernovae*, page 195.

[Hakobyan et al., 2020] Hakobyan, A. A., Barkhudaryan, L. V., Karapetyan, A. G., Gevorgyan, M. H., Mamon, G. A., Kunth, D., Adibekyan, V., and Turatto, M. (2020). Supernovae and their host galaxies - VII. The diversity of Type Ia supernova progenitors. , 499(1):1424–1440.

[Heringer et al., 2017] Heringer, E., Pritchet, C., Kezwer, J., Graham, M. L., Sand, D., and Bildfell, C. (2017). Type Ia Supernovae: Colors, Rates, and Progenitors. , 834(1):15.

[Hillebrandt and Niemeyer, 2000] Hillebrandt, W. and Niemeyer, J. C. (2000). Type IA Supernova Explosion Models. , 38:191–230.

[Hillman et al., 2016] Hillman, Y., Prialnik, D., Kovetz, A., and Shara, M. M. (2016). Growing White Dwarfs to the Chandrasekhar Limit: The Parameter Space of the Single Degenerate SNIa Channel. , 819(2):168.

[Horiuchi and Beacom, 2010] Horiuchi, S. and Beacom, J. F. (2010). Revealing Type Ia Supernova Physics with Cosmic Rates and Nuclear Gamma Rays. , 723(1):329–341.

[Iben and Tutukov, 1984] Iben, I., J. and Tutukov, A. V. (1984). Supernovae of type I as end products of the evolution of binaries with components of moderate initial mass. , 54:335–372.

[Jha et al., 2019] Jha, S. W., Maguire, K., and Sullivan, M. (2019). Observational properties of thermonuclear supernovae. *Nature Astronomy*, 3:706–716.

[Law et al., 2009] Law, N. M., Kulkarni, S. R., Dekany, R. G., Ofek, E. O., Quimby, R. M., Nugent, P. E., Surace, J., Grillmair, C. C., Bloom, J. S., Kasliwal, M. M., Bildsten, L., Brown, T., Cenko, S. B., Ciardi, D., Croner, E., Djorgovski, S. G., van Eyken, J., Filippenko, A. V., Fox, D. B., Gal-Yam, A., Hale, D., Hamam, N., Helou, G., Henning, J., Howell, D. A., Jacobsen, J., Laher, R., Mattingly, S., McKenna, D., Pickles, A., Poznanski, D., Rahmer, G., Rau, A., Rosing, W., Shara, M., Smith, R., Starr, D., Sullivan, M., Velur, V., Walters, R., and Zolkower, J. (2009). The Palomar Transient Factory: System Overview, Performance, and First Results. , 121(886):1395.

[Leaman et al., 2011] Leaman, J., Li, W., Chornock, R., and Filippenko, A. V. (2011). Nearby supernova rates from the Lick Observatory Supernova Search - I. The methods and data base. , 412(3):1419–1440.

[Li et al., 2011a] Li, W., Chornock, R., Leaman, J., Filippenko, A. V., Poznanski, D., Wang, X., Ganeshalingam, M., and Mannucci, F. (2011a). Nearby supernova rates from the Lick Observatory Supernova Search - III. The rate-size relation, and the rates as a function of galaxy Hubble type and colour. , 412(3):1473–1507.

[Li et al., 2011b] Li, W., Leaman, J., Chornock, R., Filippenko, A. V., Poznanski, D., Ganeshalingam, M., Wang, X., Modjaz, M., Jha, S., Foley, R. J., and Smith, N. (2011b). Nearby supernova rates from the Lick Observatory Supernova Search - II. The observed luminosity functions and fractions of supernovae in a complete sample. , 412(3):1441–1472.

[Li et al., 2019] Li, W., Wang, X., Vinkó, J., Mo, J., Hosseinzadeh, G., Sand, D. J., Zhang, J., Lin, H., PTSS/TNTS, Zhang, T., Wang, L., Zhang, J., Chen, Z., Xiang, D., Rui, L., Huang, F., Li, X., Zhang, X., Li, L., Baron, E., Derkacy, J. M., Zhao, X., Sai, H., Zhang, K., Wang, L., LCO, Howell, D. A., McCully, C., Arcavi, I., Valenti, S., Hiramatsu, D., Burke, J., KEGS, Rest, A., Garnavich, P., Tucker, B. E., Narayan, G., Shaya, E., Margheim, S., Zenteno, A., Villar, A., UCSC, Dimitriadis, G., Foley, R. J., Pan, Y. C., Coulter, D. A., Fox, O. D., Jha, S. W., Jones, D. O., Kasen, D. N., Kilpatrick, C. D., Piro, A. L., Riess, A. G., Rojas-Bravo, C., ASAS-SN, Shappee, B. J., Holoien, T. W. S., Stanek, K. Z., Drout, M. R., Auchettl, K., Kochanek, C. S., Brown, J. S., Bose, S., Bersier, D., Brimacombe, J., Chen, P., Dong, S., Holmbo, S., Muñoz, J. A., Mutel, R. L., Post, R. S., Prieto, J. L., Shields, J., Tallon, D., Thompson, T. A., Vallely, P. J., Villanueva, S., J., Pan-STARRS, Smartt, S. J., Smith, K. W., Chambers, K. C., Flewelling, H. A., Huber, M. E., Magnier, E. A., Waters, C. Z., Schultz, A. S. B., Bulger, J., Lowe, T. B., Willman, M., Konkoly/Texas, Sárneczky, K., Pál, A., Wheeler, J. C., Bódi, A., Bognár, Z., Csák, B., Cseh, B., Csörnyei, G., Hanyecz, O., Ignácz, B., Kalup, C., Könyves-Tóth, R., Kriskovics, L., Ordasi, A., Rajmon, I., Sódor, A., Szabó, R., Szakáts, R., Zsidi, G., Arizona, U. o., Milne, P., Andrews, J. E., Smith, N., Bilinski, C., Swift, Brown, P. J., ePESSTO, Nordin, J., Williams, S. C., Galbany, L., Palmerio, J., Hook, I. M., Inserra, C., Maguire, K., Cartier, R., Razza, A., Gutiérrez, C. P., North Carolina, U. o., Hermes, J. J., Reding, J. S., Kaiser, B. C., ATLAS, Tonry, J. L., Heinze, A. N., Denneau, L., Weiland, H., Stalder, B., K2 Mission Team, Barentsen, G., Dotson, J., Barclay, T., Gully-Santiago, M., Hedges, C., Cody, A. M., Howell, S., Kepler Spacecraft Team, Coughlin, J., Van Cleve, J. E., Cardoso, J. V. d. M., Larson, K. A., McCalmont-Everton, K. M., Peterson, C. A., Ross, S. E., Reedy, L. H., Osborne, D., McGinn, C., Kohnert, L., Migliorini, L., Wheaton, A., Spencer, B., Labonde, C., Castillo, G., Beerman, G., Steward, K., Hanley, M., Larsen, R., Gangopadhyay, R., Kloetzel, R., Weschler, T., Nystrom, V., Moffatt, J., Redick, M., Griest, K., Packard, M., Muszynski, M., Kampmeier, J., Bjella, R., Flynn, S., and Elsaesser, B. (2019). Photometric and Spectroscopic Properties of Type Ia Supernova 2018oh with Early Excess Emission from the Kepler 2 Observations. , 870(1):12.

[Livio and Mazzali, 2018] Livio, M. and Mazzali, P. (2018). On the progenitors of Type Ia supernovae. , 736:1–23.

[Makarov et al., 2014] Makarov, D., Prugniel, P., Terekhova, N., Courtois, H., and Vauglin, I. (2014). HyperLEDA. III. The catalogue of extragalactic distances. , 570:A13.

[Maoz et al., 2014] Maoz, D., Mannucci, F., and Nelemans, G. (2014). Observational Clues to the Progenitors of Type Ia Supernovae. , 52:107–170.

[Mazzali et al., 2007] Mazzali, P. A., Röpke, F. K., Benetti, S., and Hillebrandt, W. (2007). A Common Explosion Mechanism for Type Ia Supernovae. *Science*, 315(5813):825.

[Nomoto et al., 2013] Nomoto, K., Kobayashi, C., and Tominaga, N. (2013). Nucleosynthesis in stars and the chemical enrichment of galaxies. *Annual Review of Astronomy and Astrophysics*, 51(1):457–509.

[Nomoto et al., 2007] Nomoto, K., Saio, H., Kato, M., and Hachisu, I. (2007). Thermal Stability of White Dwarfs Accreting Hydrogen-rich Matter and Progenitors of Type Ia Supernovae. , 663(2):1269–1276.

[Pâris et al., 2017] Pâris, I., Petitjean, P., Ross, N. P., Myers, A. D., Aubourg, É., Streblyanska, A., Bailey, S., Armengaud, É., Palanque-Delabrouille, N., Yèche, C., Hamann, F., Strauss, M. A., Albareti, F. D., Bovy, J., Bizyaev, D., Niel Brandt, W., Brusa, M., Buchner, J., Comparat, J., Croft, R. A. C., Dwelly, T., Fan, X., Font-Ribera, A., Ge, J., Georgakakis, A., Hall, P. B., Jiang, L., Kinemuchi, K., Malanushenko, E., Malanushenko, V., McMahon, R. G., Menzel, M.-L., Merloni, A., Nandra, K., Noterdaeme, P., Oravetz, D., Pan, K., Pieri, M. M., Prada, F., Salvato, M., Schlegel, D. J., Schneider, D. P., Simmons, A., Viel, M., Weinberg, D. H., and Zhu, L. (2017). The Sloan Digital Sky Survey Quasar Catalog: Twelfth data release. , 597:A79.

[Parrent et al., 2014] Parrent, J., Friesen, B., and Parthasarathy, M. (2014). A review of type Ia supernova spectra. , 351(1):1–52.

[Perlmutter et al., 1999] Perlmutter, S., Aldering, G., Goldhaber, G., Knop, R. A., Nugent, P., Castro, P. G., Deustua, S., Fabbro, S., Goobar, A., Groom, D. E., Hook, I. M., Kim, A. G., Kim, M. Y., Lee, J. C., Nunes, N. J., Pain, R., Pennypacker, C. R., Quimby, R., Lidman, C., Ellis, R. S., Irwin, M., McMahon, R. G., Ruiz-Lapuente, P., Walton, N., Schaefer, B., Boyle, B. J., Filippenko, A. V., Matheson, T., Fruchter, A. S., Panagia, N., Newberg, H. J. M., Couch, W. J., and Project, T. S. C. (1999). Measurements of Ω and Λ from 42 High-Redshift Supernovae. , 517(2):565–586.

[Phillips, 1993] Phillips, M. M. (1993). The Absolute Magnitudes of Type IA Supernovae. , 413:L105.

[Pritchet et al., 2008] Pritchet, C. J., Howell, D. A., and Sullivan, M. (2008). The Progenitors of Type Ia Supernovae. , 683(1):L25.

[Riess et al., 2019] Riess, A. G., Casertano, S., Yuan, W., Macri, L. M., and Scolnic, D. (2019). Large Magellanic Cloud Cepheid Standards Provide a 1% Foundation for the Determination of the Hubble Constant and Stronger Evidence for Physics beyond ΛCDM. , 876(1):85.

[Riess et al., 1998] Riess, A. G., Filippenko, A. V., Challis, P., Clocchiatti, A., Diercks, A., Garnavich, P. M., Gilliland, R. L., Hogan, C. J., Jha, S., Kirshner, R. P., Leibundgut, B., Phillips, M. M., Reiss, D., Schmidt, B. P., Schommer, R. A., Smith, R. C., Spyromilio, J., Stubbs, C., Suntzeff, N. B., and Tonry, J. (1998). Observational Evidence from Supernovae for an Accelerating Universe and a Cosmological Constant. , 116(3):1009–1038.

[Röpke and Hillebrandt, 2005] Röpke, F. K. and Hillebrandt, W. (2005). On the Stability of Thermonuclear Burning Fronts in Type Ia Supernovae. In Marcaide, J.-M. and Weiler, K. W., editors, *IAU Colloq. 192: Cosmic Explosions, On the 10th Anniversary of SN1993J*, volume 99, page 333.

[Ruiter et al., 2009] Ruiter, A. J., Belczynski, K., and Fryer, C. (2009). Rates and Delay Times of Type Ia Supernovae. , 699(2):2026–2036.

[Sato et al., 2015] Sato, Y., Nakasato, N., Tanikawa, A., Nomoto, K., Maeda, K., and Hachisu, I. (2015). A Systematic Study of Carbon-Oxygen White Dwarf Mergers: Mass Combinations for Type Ia Supernovae. , 807(1):105.

[Silverman et al., 2013] Silverman, J. M., Ganeshalingam, M., and Filippenko, A. V. (2013). Berkeley Supernova Ia Program - V. Late-time spectra of Type Ia Supernovae. , 430(2):1030–1041.

[Skrutskie et al., 2006] Skrutskie, M. F., Cutri, R. M., Stiening, R., Weinberg, M. D., Schneider, S., Carpenter, J. M., Beichman, C., Capps, R., Chester, T., Elias, J., Huchra, J., Liebert, J.,

Lonsdale, C., Monet, D. G., Price, S., Seitzer, P., Jarrett, T., Kirkpatrick, J. D., Gizis, J. E., Howard, E., Evans, T., Fowler, J., Fullmer, L., Hurt, R., Light, R., Kopan, E. L., Marsh, K. A., McCallon, H. L., Tam, R., Van Dyk, S., and Wheelock, S. (2006). The Two Micron All Sky Survey (2MASS). , 131(2):1163–1183.

[Taubenberger, 2017] Taubenberger, S. (2017). *The Extremes of Thermonuclear Supernovae*, page 317.

[Taubenberger et al., 2015] Taubenberger, S., Elias-Rosa, N., Kerzendorf, W. E., Hachinger, S., Spyromilio, J., Fransson, C., Kromer, M., Ruiter, A. J., Seitenzahl, I. R., Benetti, S., Cappellaro, E., Pastorello, A., Turatto, M., and Marchetti, A. (2015). Spectroscopy of the Type Ia supernova 2011fe past 1000d. , 448:L48–L52.

[Webbink, 1984] Webbink, R. F. (1984). Double white dwarfs as progenitors of R Coronae Borealis stars and type I supernovae. , 277:355–360.

[Whelan and Iben, 1973] Whelan, J. and Iben, Icko, J. (1973). Binaries and Supernovae of Type I. , 186:1007–1014.

[White et al., 2011] White, D. J., Daw, E. J., and Dhillon, V. S. (2011). A list of galaxies for gravitational wave searches. *Classical and Quantum Gravity*, 28(8):085016.

[Wolf et al., 2013] Wolf, W. M., Bildsten, L., Brooks, J., and Paxton, B. (2013). Hydrogen Burning on Accreting White Dwarfs: Stability, Recurrent Novae, and the Post-nova Supersoft Phase. , 777(2):136.